European Journal of Mechanics / A Solids 99 (2023) 104950

Contents lists available at ScienceDirect

European Journal of Mechanics / A Solids

journal homepage: www.elsevier.com/locate/ejmsol

# Pullout characteristics of functionally graded and degraded adhesive anchors

S. Kumar [a,b,*], M.A. Khan [c], Brian L. Wardle [d,e], J.N. Reddy [f]

[a] Materials & Manufacturing Research Group, James Watt School of Engineering, University of Glasgow, Glasgow G12 8QQ, UK
[b] Glasgow Engineering Computational Centre, James Watt School of Engineering, University of Glasgow, Glasgow G12 8LT, UK
[c] Department of Civil Engineering, Mahindra University, Ecole Centrale School of Engineering, Bahadurpally, Hyderabad 500043, India
[d] Department of Aeronautics & Astronautics, Massachusetts Institute of Technology, 77 Massachusetts Avenue, Cambridge, MA 02139-4307, USA
[e] Department of Mechanical Engineering, Massachusetts Institute of Technology, 77 Massachusetts Avenue, Cambridge, MA 02139-4307, USA
[f] J. Mike Walker '66 Department of Mechanical Engineering, Texas A&M University, College Station, TX 77843-3123, USA

ARTICLE INFO

*Keywords:*
Adhesive anchors
Pullout strength
Debonding
Inhomogeneous bondlayer
Stress-transfer
Tailored adhesive
Layered materials/composites
Interfacial stresses

ABSTRACT

Three-dimensional axisymmetric elasticity solutions for pull-out stresses in bonded anchors with spatially stiffness-varying adhesive are presented. A stiff rod embedded in a semi-infinite rigid half-space through an adhesive bondlayer, representing a general anchor problem is analyzed. The adhesive layer is considered to have a smoothly varying stiffness over embedded length. Two cases of particular engineering relevance are considered: (i) stiffness grading of the bondlayer to enhance performance while retaining the critical length characteristics of bonded anchors, and (ii) modulus reduction of the bondlayer representing adhesive degradation proximal to the loaded-end. Theoretical solutions are developed adopting a stress function approach in conjunction with a variational method that compare well with 3D axisymmetric finite element (FE) results. Both theoretical and FE results indicate that the maximum shear stress in the adhesive decreases over 60% for a graded bondlayer for the parameters considered here without warranting a longer embedment length. In contrast, the degraded bondlayer reduces shear stress peaks significantly but warrants a larger embedment length to enable shear-dominated stress-transfer, disadvantageously loading the embedded-end in tension. A design map showing the critical embedment length required for degraded bondlines as a function of fractional embedment length over which bondline is regarded to have degraded is presented. In addition, interfacial fracture behaviors of the tailored and degraded adhesive anchors were examined through FE analyses finding that the tailoring reduces the energy release rate and has the potential for enhancing damage tolerance. The findings of the study indicate that the stiffness-tailored and -degraded bondlayers significantly redistribute the stress field with concomitant influence on stress-transfer and interfacial debonding characteristics of bonded anchors.

## 1. Introduction

The stress-transfer between the fiber and the matrix in fiber reinforced composites in the neighborhood of a fiber break while there is perfect bonding at the fiber–matrix interface is an important mechanics problem (McCartney, 1989; Cox, 1952; Nairn, 1997) as it is applicable to several different situations. Therefore, in this study, the generic problem of load-transfer between a broken fiber bonded to the matrix is investigated and discussed in the context of adhesively bonded anchors, ubiquitous in construction industry. Retrofitting and rehabilitation of aging infrastructure as well as the demand for flexibility in utilizing the existing structures has led to an increased usage of fastening systems. Adhesively bonded structural systems have been widely adopted for such applications because of their rapid curing speed and cost-effectiveness (Upadhyaya and Kumar, 2015b; Kalfat and Al-Mahaidi, 2015). Four different modes of failure have been reported for adhesive anchors (Cook, 1993): (i) debonding of the anchor-adhesive or adhesive-concrete interface occurs at the embedded-end of the anchor when tensile stress reaches the interface tensile strength of the adhesive; (ii) debonding of the anchor-adhesive or the adhesive-concrete interface occurs due to shearing of lateral surface of the adhesive for anchors with thin adhesive layer and larger embedment length; (iii) concrete failure (concrete-cone failure) occurs when the embedment length is small (between 3 to 5 times of the diameter of the anchor); and (iv) the failure of anchor (rod breakage) occurs when the tensile stress in the anchor rod exceeds its tensile strength. The experimental work by Zavliaris et al. (1996), observed bond-failure for embedment lengths in the range of 8.3 to 10 times the anchor diameter and the failure of anchor is noted for an embedment length of about 11.2 times

* Corresponding author at: Glasgow Engineering Computational Centre, James Watt School of Engineering, University of Glasgow, Glasgow G12 8LT, UK.
*E-mail addresses:* s.kumar@eng.oxon.org, msv.kumar@glasgow.ac.uk (S. Kumar).

https://doi.org/10.1016/j.euromechsol.2023.104950
Received 24 October 2022; Received in revised form 11 February 2023; Accepted 12 February 2023
Available online 20 February 2023

the diameter of anchor, for a bondline thickness in the range of 2 to 4 mm. The design specifications for industrial anchors recommend larger embedment lengths with a thin adhesive. Therefore, the pullout failure mode is very important in such a scenario (Upadhyaya and Kumar, 2015b; Kumar and Khan, 2016b).

Several theoretical, experimental, and numerical studies have reported pullout performance of anchors with non-tailored bondlayer (see for instance, McVay et al. (1996), Farmer (1975), Kim and Smith (2010), Cook (1993), Wang et al. (2020)). The works of Cook (1993), Cook and Konz (2001) and Doerr and Klingner (1989) provided an in-depth analysis of the failure characteristics of adhesive anchors. To assess the non-uniform bond-stress in adhesively bonded anchors with homogeneous adhesive, shear-lag elastic analysis was utilized, neglecting the influence of Poisson's ratio of the bondline (Cook et al., 1993; Farmer, 1975). A thorough analysis of models for concrete-cone, bond, and combined failure modes, as well as calibrated models for FRP spike anchors based on trials and existing models, were reported by Kim and Smith (2010). Some of the above models assumed a uniform bond-stress and therefore, spatial variation of shear stress and other possible failure modes were ignored.

The analytical work of Chen et al. (2015) on cable bolted anchors, showcased that for anchors with a larger embedment length, the shear stress distribution along the interface is non-uniform. Prieto-Muñoz et al. (2013a) proposed closed form elastic solutions for stresses in adhesively bonded anchors and compared the results with an axisymmetric finite element solution. They further extended the models to account for the visco-elastic behavior of the adhesive (Prieto-Muñoz et al., 2013b). Recent studies (Upadhyaya and Kumar, 2015b; Kumar and Khan, 2016b; Khan et al., 2022) demonstrated that the boundary condition at the embedded-end of the anchor has a negligible influence on the shear stress distribution and its peak for practical anchors with larger embedment length and stiff adhesive. This is because the embedment length considered is long enough for shear-dominated stress-transfer through the adhesive eventhough the embedded-end is intact and has the potential to transfer the load in direct tension. Therefore, the boundary condition at the embedded-end may not influence the failure mode/characteristics of practical adhesive anchors as long as the strength and stiffness of the adhesive remains unchanged with time. Wang et al. (2020) proposed a 3D analytical solution in contrast to a one dimensional model which we refer to as a shear-lag model, for predicting the performance of bonded anchors with non-tailored bondlayer. They also reported that a majority of studies rely on shear-lag analysis for predicting the pullout performance of bonded anchors with non-tailored bondlayer.

Theoretical analyses of stress-transfer in unidirectional fiber reinforced composites (see for e.g., Nairn (1997), Upadhyaya and Kumar (2015a)) and stress-transfer through partially debonded interfaces in three-phase composites (Wu et al., 1998, 1999) provide potential guidance for analyzing pullout performance and interfacial debonding behavior of adhesive anchors due to similar nature of these problems. In an effort to understand the stress-transfer through the adhesive interfaces, several analytical solutions have been proposed for bonded systems (Yang et al., 2008; Ballarini et al., 1986; Gesoğlu et al., 2014; Steen and Valles, 1998).

Adhesive interfaces with spatially-varying stiffness deserve attention from the standpoint of designing efficient bonded anchors so as to improve their pullout capacity and damage tolerance (Krasucki and Lenci, 2000). Several studies (Stein et al., 2017; Khan et al., 2018; Paroissien et al., 2018) proposed theoretical models for bonded joints with functionally graded adhesive to predict the effect of such stiffness-grading on reduction in peak adhesive stresses. Finite element studies with continuum damage models were conducted by Kim et al. (2021) to evaluate mixed-mode failure characteristics of functionally graded adhesive joints. Recent studies and surveys on functionally graded adhesive joints provide insights into the analysis, fabrication, experimental testing and applications of interface-tailored joints (Durodola, 2017; Kumar and Adams, 2017; Stapleton et al., 2021). For instance, Stapleton et al. (2012) used glass beads with variable volume fraction to tailor the adhesive stiffness over the bondlength of a single-lap joint. Furthermore, second generation acrylic adhesive could be tailored by changing the mixing ratios (Sekiguchi et al., 2019). Recently, manufacturing challenges in realizing spatially tailored adhesives were discussed by Marques et al. (2021). Dadian and Rahnama (2021) has reported a remarkable improvement ($\approx$ 300%) in shear load-carrying capacity of joint due to an optimal tailoring of adhesive. Functionally graded adhesives have already been employed in bonded repairs (Bouchikhi et al., 2010; Kim et al., 2013). Emerging multi-material 3D printing techniques also facilitate the fabrication of such stiffness-tailored bondlayers/interfaces (Kumar et al., 2016, 2018; Khan and Kumar, 2018) and adherends (Ubaid et al., 2018).

Degradation of the epoxy adhesive along with its creep deformation led to the fatal collapse of a suspended ceiling section in the Interstate 90 Connector Tunnel in Boston, Massachusetts on July 10th 2006 (NTSB, 2007). This has sparked enormous research interest in predicting the loss of strength and stiffness of the adhesive material and the performance of the adhesively bonded anchors under sustained loading (Kränkel et al., 2015). Under appropriate service condition, the embedded-end of the anchor is perfectly bonded to the concrete through adhesive. In this case, the embedded-end of the anchor is regarded to be fully restrained by the concrete. On the other hand, if either the concrete has fractured, or alternatively, the hole at the embedded-end is dry due to non-penetration of adhesive this far, this restraint would be zero. The latter can occur due to deficient installation. Non-linear irreversible creep deformations of the adhesives, stress level and the operating conditions such as the presence of moisture or freeze-thaw cycles as well as off-design cure cause degradation of the adhesives, leading to spatially varying-stiffness of the bondline as a function of time (Rizzoni and Lebon, 2013; Tipireddy and Kumar, 2017). This renders the bondline compliant. Decrease in stiffness of the bondline warrants a larger embedment length for complete shear stress-transfer (Tipireddy and Kumar, 2017). The peak shear stress in the bondlayer is always higher for the case of anchors with debonded embedded-end (Khan et al., 2022; Kumar and Khan, 2016b). Therefore, considering debonded-interface condition at the embedded-end of the anchor is indispensable to assess the influence of bondline stiffness-degradation on the pullout strength and interfacial fracture behavior of such systems. Furthermore, as reported by authors' previous work (Khan et al., 2022), the critical length anchors show a zero shear stress in the adhesive at the debonded embedded-end while they show finite tensile stress at the embedded-end for anchors with perfectly bonded embedded-end. As the embedded-end condition is uncertain, for a conservative design, we consider debonded embedded-end to evaluate stresses and to identify critical transfer length $l_{cr}$. Note that $l_{cr}$ is the minimum length required for shear-dominated load transfer and the anchors with shorter embedment length exhibit concrete-failure rather than a bond-failure.

Therefore, this study is focused on the stress-transfer and interfacial debonding characteristics of adhesive anchors subjected to a pullout load, considering spatial variation in bondline stiffness over a partial/entire embedment length via a theoretical framework, adopting a stress function approach in conjunction with a variational method, in contrast to a shear-lag analysis adopted by the previous studies. In this line of view, a 3D analytical solution for stress-transfer is proposed for the bonded anchors with functionally stiffness-varying adhesive subjected to a pullout load. The novelty of the proposed model is that it accounts for a complex stress-state in the bonded anchors with graded bondlines rather than employing a shear-lag model which ignores the Poisson's effect. To the best of authors' knowledge only one model capable of capturing such a complex stress-state exists for the analysis of anchors, that too, with homogeneous bondline (Wang et al., 2020). Therefore, in this study, we propose a model to analyze the stress-transfer characteristics in the functionally graded anchors

considering a 3D axisymmetric formulation. Moreover, as demonstrated by Wang et al. (2020), strength prediction based on a 3D axisymmetric formulation is more accurate than the shear-lag model. The first part of the study investigates the effect of a tailored bondline in reducing shear stress concentrations in the bonded anchors, while the subsequent part of this study evaluates the stress distribution in a degraded bondline. Finally, this study investigates the interfacial debonding characteristics of bonded anchors with homogeneous, tailored and degraded bondlines.

## 2. Analytical model

Consider an anchor rod of radius $a$ embedded in a semi-infinite concrete half-space over a length $l$ through an adhesive layer of internal and external radii $a$ and $b$, respectively, as shown in Fig. 1a. The anchor is considered either as a transversely isotropic or an isotropic linear-elastic material, while the adhesive is regarded as a linear elastic isotropic continuum. Note that the transverse isotropy of the anchor allows for the generalization of proposed model to the cases of fiber–matrix pullout studies. The interface between the bonded-in end of the anchor and the concrete is assumed to be completely debonded/unbonded as shown in Fig. 1a. The axisymmetric assembly is referred to a cylindrical coordinate system $(r, \theta, z)$, representing radial, circumferential and longitudinal directions respectively, with origin $O$ at the bonded-in end of the anchor as shown in Fig. 1a. The anchor rod is subjected to an axial tensile load $P$ as shown in Fig. 1a. $\sigma_0$ is the axial tensile stress experienced by the anchor due to applied load $P$ at $z = l$ and therefore $\sigma_0 = \frac{P}{\pi a^2}$. $E_i$ and $\nu_i$ denote the Young's modulus and the Poisson's ratio of the member $i$, respectively. $l_c$ is the critical length required for shear-dominated stress-transfer. Fig. 1b shows modulus profiles ($E_2(z)$) considered for homogeneous, tailored and degraded bondlines over the embedment length. $E_m$ is the Young's modulus of the homogeneous adhesive. $E_p$ and $E_0$ are the maximum and minimum Young's moduli respectively of the tailored bondline whose effective modulus is $E_m$. $E_m$ and $E_d$ are the maximum and minimum Young's moduli of the partially degraded bondline respectively. For representing partially degraded bondline, adhesive modulus is de-graded near the loaded end over $(1-\zeta)l \le z \le l$ such that $0 < \zeta < 1$. Fig. 1c shows typical interfacial shear stress distribution over the embedded length for different modulus profiles considered in Fig. 1b. Note that $l_c$ required for both tailored bondline and homogeneous bondlines with modulus $E_m$ are the same to ensure shear-dominated load transfer from the anchor/fiber to the adhesive/matrix as the effective stiffness of the tailored bondline is $E_m$.

The following assumptions have been adopted in order to develop a tractable analytical model.

- The radial stress in each member is assumed to be proportional to circumferential stress (Kumar and Khan, 2016a) such that $\sigma_{rr}^{(i)}(r,z) = \lambda_i\, \sigma_{\theta\theta}^{(i)}(r,z)$, where $\lambda_i$ is a proportionality constant of the member '$i$'. The superscript/subscript $i$=1 for anchor and $i = 2$ for adhesive layer.
- The anchor, adhesive layer and the concrete are assumed to be perfectly bonded at their respective lateral interfaces.
- Axial stress in each member is assumed to spatially vary along the '$z$' coordinate only, i.e., $\sigma_{zz}^{(1)} = \sigma_{zz}^{(1)}(z)$ ; $\sigma_{zz}^{(2)} = \sigma_{zz}^{(2)}(z)$. For brevity, we henceforth denote $\sigma_{zz}^{(i)}$ by $\sigma_i$.
- Adhesive layer is considered either as a homogeneous or an inhomogeneous linear elastic isotropic material such that $E_2$ is either a constant or a function of $z$ i.e., $E_2(z)$.
- The concrete is relatively stiffer (~ 10–15 times) than the bulk adhesive material, so the deformation of an anchor under a pullout load is mainly caused by the deformation of adhesive layer and therefore the concrete is assumed to be infinitely stiff (Upadhyaya and Kumar, 2015b).

### 2.1. Stress field

The axisymmetric equilibrium equations considering $\sigma_{rr}^{(i)} = \sigma_{\theta\theta}^{(i)}$ for each of the members taking $\lambda_i = 1$ can be written as:

$$\frac{\partial}{\partial r}(r\sigma_{rz}^{(i)}) + r\frac{\partial \sigma_{zz}^{(i)}}{\partial z} = 0 \tag{1}$$

$$\frac{\partial}{\partial r}(r\sigma_{rr}^{(i)}) + r\frac{\partial \sigma_{rz}^{(i)}}{\partial z} - \sigma_{rr}^{(i)} = 0 \tag{2}$$

Admissible stress fields are derived from the equilibrium equations of the system given above using traction-free boundary conditions, stress continuity conditions at the anchor-adhesive interface and rigid adhesive-concrete interface condition. Using equilibrium Eq. (1), an implicit expression for the shear stress in the anchor rod can be written as:

$$r\sigma_{rz}^{(1)} = -\frac{r^2}{2}\dot{\sigma}_1 + \chi_1 \tag{3}$$

where, $\dot{\sigma}_1 = \frac{d\sigma_1}{dz}$. At the center of the anchor, shear stress is zero as it is the axis of symmetry i.e., $\sigma_{rz}^{(1)}(0,z)$=0 and this yields $\chi_1$=0. Therefore, the shear stress in the anchor is given by

$$\sigma_{rz}^{(1)} = -\frac{r}{2}\dot{\sigma}_1 \quad ; \qquad 0 \le r \le a \tag{4}$$

Using equilibrium Eq. (2), and Eq. (4), radial stress in the anchor is expressed as:

$$\sigma_{rr}^{(1)} = \frac{r^2}{4}\ddot{\sigma}_1 + \chi_2(z) \tag{5}$$

where, $\ddot{\sigma}_1 = \frac{d^2\sigma_1}{dz^2}$. Without loss of generality, it can be assumed that $\sigma_{rr}^{(1)}(0,z) = k\ \ddot{\sigma}_1$. This gives $\chi_2 = k\ddot{\sigma}_1$. Therefore, radial stress in the anchor is given by

$$\sigma_{rr}^{(1)} = \left(\frac{r^2}{4} + k\right)\ddot{\sigma}_1 \quad ; \quad 0 \le r \le a \tag{6}$$

where, $k$ is an unknown constant to be determined. Using equilibrium Eq. (1), we get

$$r\sigma_{rz}^{(2)} = -\frac{r^2}{2}\dot{\sigma}_2 + r\ \chi_3 + \chi_4(z) \tag{7}$$

Using shear stress continuity condition at the anchor-adhesive interface and global axial equilibrium condition given respectively by

$$\sigma_{rz}^{(2)}(a,z) = \sigma_{rz}^{(1)}(a,z) \quad ; \quad \pi a^2\sigma_o = \int_0^l \sigma_{rz}^{(2)}(b,z)\ 2\pi b\ dz \tag{8}$$

we get, $\chi_3 = 0$ and $\chi_4 = \frac{a^2}{2}\left(\dot{\sigma}_2 - \dot{\sigma}_1\right)$. Therefore, the shear stress in the adhesive layer is expressed as:

$$\sigma_{rz}^{(2)} = \frac{(a^2 - r^2)}{2r}\ \dot{\sigma}_2 - \frac{a^2}{2r}\ \dot{\sigma}_1 \quad ; \qquad a \le r \le b \tag{9}$$

where, $\dot{\sigma}_2 = \frac{d\sigma_2}{dz}$. Using equilibrium Eqs. (2) and (9), the radial stress in the adhesive can be derived as:

$$\sigma_{rr}^{(2)} = \left(\frac{r^2}{4} - \frac{a^2}{2}ln(r)\right)\ddot{\sigma}_2 + \frac{a^2}{2}ln(r)\ \ddot{\sigma}_1 + \chi_5(z)\ r + \chi_6(z) \tag{10}$$

Since, the lateral surface of the adhesive is restrained by the stiff concrete, we consider that the hoop strain at the adhesive-concrete interface to be zero i.e $\varepsilon_{\theta\theta}^{(2)}(b,z) = 0$ such that

$$\sigma_{rr}^{(2)}(b,z) = \frac{\nu_2}{(1-\nu_2)}\sigma_2 \tag{11}$$

Considering radial stress continuity condition at the anchor-adhesive interface i.e., $\sigma_{rr}^{(2)}(a,z) = \sigma_{rr}^{(1)}(a,z)$ and using Eq. (11), we deduce

$$\chi_5(z) = \xi\ddot{\sigma}_1 - \rho\sigma_2 - \beta\ddot{\sigma}_2 \tag{12}$$

and

$$\chi_6(z) = -\left(\frac{a^2}{2}ln(b) + b\xi\right)\ddot{\sigma}_1 + \left(\frac{\nu_2}{1-\nu_2} + b\rho\right)\sigma_2 + \left(\frac{a^2}{2}ln(b) - \frac{b^2}{4} + b\beta\right)\ddot{\sigma}_2$$

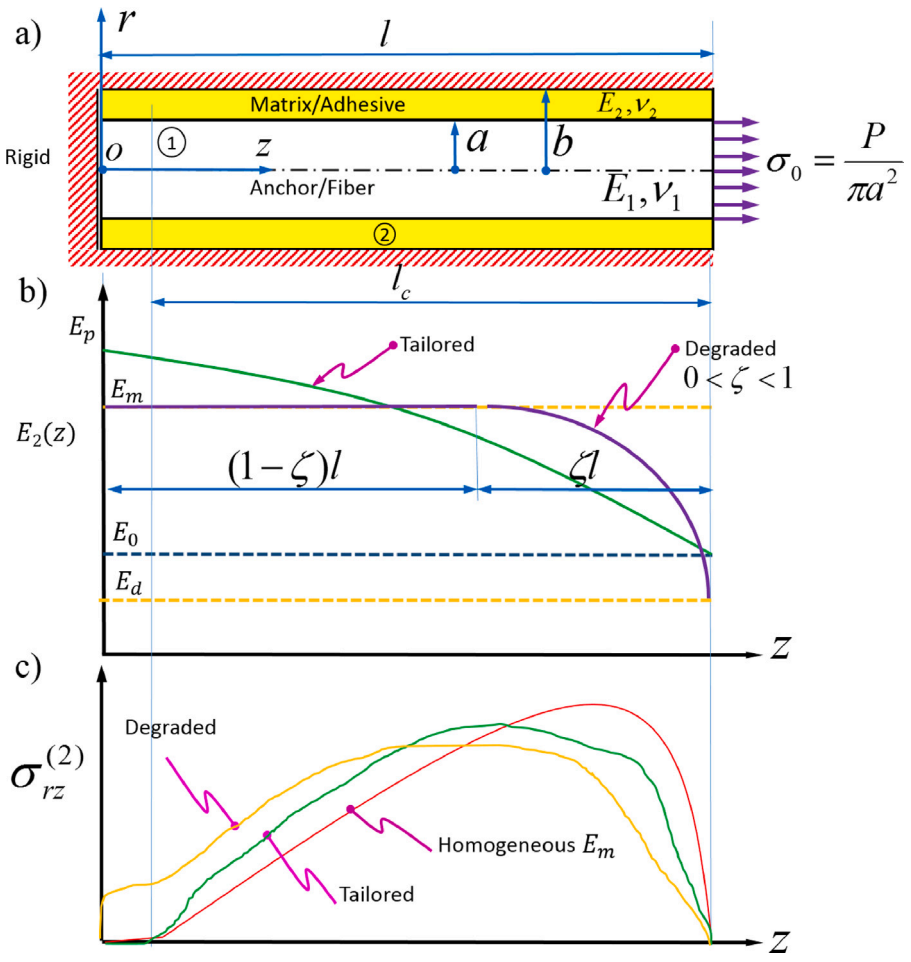


**Fig. 1.** A. Adhesive anchor embedded in rigid half-space b. Elastic modulus profile for tailored, homogeneous and degraded bondlines ($E_2(z)$) over the embedment length. $E_m$ is the Young's modulus of the homogeneous adhesive. $E_p$ and $E_0$ are the maximum and minimum Young's moduli of the tailored bondline respectively whose effective modulus is $E_m$. $E_m$ and $E_d$ are the maximum and minimum Young's moduli of the partially degraded bondline respectively. For partially degraded bondline, adhesive modulus is graded over $(1-\zeta)l \le z \le l$ such that $0 < \zeta < 1$. d. Typical adhesive shear stress distribution over the embedded length for different modulus profiles when anchor/fiber is subjected a pullout stress $\sigma_0$. $P$ is the tensile load applied to anchor at $z = l$.

(13)

The radial stress in the adhesive layer is therefore given by

$$\begin{aligned}\sigma_{rr}^{(2)} &= k\left(\frac{(r-b)}{(a-b)}\right)\ddot{\sigma}_1 + \left(\frac{a^2}{2}ln\left(\frac{r}{b}\right) + \xi(r-b)\right)\ddot{\sigma}_1 \\ &+ \left(\frac{\nu_2}{1-\nu_2} + \rho(b-r)\right)\sigma_2 \\ &+ \left(\frac{a^2}{2}ln\left(\frac{b}{r}\right) + \frac{(r^2-b^2)}{4} + \beta(b-r)\right)\ddot{\sigma}_2 \quad ; \qquad a \le r \le b \end{aligned} \tag{14}$$

where, the known constants $\xi$, $\rho$ and $\beta$ depend on the geometric and/or material properties of the bonded anchorage and are given in the Appendix A. For the anchor, 3D axisymmetric constitutive relations for linear-elastic homogeneous material considering $\sigma_{rr}^{(1)} = \sigma_{\theta\theta}^{(1)}$ are:

$$\begin{aligned}&\varepsilon_{rr}^{(1)} = \frac{(1-\nu_1)}{E_1}\sigma_{rr}^{(1)} - \frac{\nu_1}{E_1}\sigma_{zz}^{(1)}; \quad \varepsilon_{zz}^{(1)} = \frac{(1-\nu_1)}{E_1}\sigma_{zz}^{(1)} - \frac{\nu_1}{E_1}\sigma_{rr}^{(1)}; \\ &\varepsilon_{rz}^{(1)} = \frac{(1+\nu_1)}{E_1}\sigma_{rz}^{(1)}\end{aligned} \tag{15}$$

Constitutive relations for linear-elastic isotropic but inhomogeneous adhesive considering $\sigma_{rr}^{(2)} = \sigma_{\theta\theta}^{(2)}$ are:

$$\begin{aligned}&\varepsilon_{rr}^{(2)} = \frac{(1-\nu_2)}{E_2(z)}\sigma_{rr}^{(2)} - \frac{\nu_2}{E_2(z)}\sigma_{zz}^{(2)}; \quad \varepsilon_{zz}^{(2)} = \frac{(1-\nu_2)}{E_2(z)}\sigma_{zz}^{(2)} - \frac{\nu_2}{E_2(z)}\sigma_{rr}^{(2)}; \\ &\varepsilon_{rz}^{(2)} = \frac{(1+\nu_2)}{E_2(z)}\sigma_{rz}^{(2)}\end{aligned} \tag{16}$$

where, $E_2(z)$ is the position dependent Young's modulus of the inhomogeneous bondline. The complementary energy density in this linear elastic assembly is given by

$$\tilde{U} = \int_0^{\sigma_{mn}^{(1)}} \varepsilon_{mn}^{(1)}\, d\sigma_{mn}^{(1)} + \int_0^{\sigma_{mn}^{(2)}} \varepsilon_{mn}^{(2)}\, d\sigma_{mn}^{(2)}$$

where, $\sigma_{mn}^{(i)}(r,z)$ is the Cauchy or nominal stress tensor at a material point in the member '$i$' and $\epsilon_{mn}^{(i)}(r,z)$ is the Lagrangian or infinitesimal strain tensor at a material point in member '$i$'. Here $m$ and $n$ independently range over $r$, $\theta$ and $z$. Using the constitutive relations given by Eq. (15), the complementary energy in the anchor is expressed as

$$U_1 = \pi \int_0^l \int_0^a \left(k_1\, {\sigma_{rr}^{(1)}}^2 r + k_2\, \sigma_1^2 r + k_3\, \sigma_{rr}^{(1)}\sigma_1 r + k_4\, {\sigma_{rz}^{(1)}}^2 r\right) dr\, dz \tag{17}$$

where, the constants $k_i (i = 1...4)$ depend upon elastic properties of anchor and are given in Appendix A. Plugging in expressions for the stress components derived above, the complementary energy in an anchor, $U_1$ could be written as

$$U_1 = \pi \int_0^l \left((A_1 + k^2 A_2 + k\, A_3)\ddot{\sigma}_1^2 + A_4\sigma_1^2 + (A_5 + k\, A_6)\sigma_1\ddot{\sigma}_1 + A_7\dot{\sigma}_1^2\right) dz \tag{18}$$

The explicit expressions for the constants $A_i (i = 1...7)$ are given in the Appendix A. Similarly, the complementary energy in a graded adhesive

layer is given by

$$U_2 = \pi \int_0^l \int_a^b \left( \eta_1 \ \sigma_{rr}^{(2)^2} r + \eta_2 \ \sigma_2^2 r + \eta_3 \ \sigma_r^{(2)} \sigma_2 r + \eta_4 \ \sigma_{rz}^{(2)^2} r \right) dr \ dz \tag{19}$$

where, the variable coefficients $\eta_i(z)(i = 1...4)$ that depend on inhomogeneous elastic properties of the adhesive are given in Appendix B. Inserting stress components for the adhesive layer in the above, we get

$$\begin{aligned} U_2 = \pi \int_0^l \Big[ & (k^2 B_1 + B_2 + k B_3)\ddot{\sigma}_1^2 + (B_4 + B_{11} + B_{14})\sigma_2^2 \\ & + B_5 \ddot{\sigma}_2^2 + (B_6 + B_{15})\sigma_2 \ddot{\sigma}_2 \\ & + (k B_7 + B_9 + k B_{12} + B_{13})\sigma_2 \ddot{\sigma}_1 + (k B_8 + B_{10})\ddot{\sigma}_1 \ddot{\sigma}_2 \\ & + B_{16}\dot{\sigma}_1^2 + B_{17}\dot{\sigma}_1^2 + B_{18}\dot{\sigma}_1 \dot{\sigma}_2 \Big] \ dz \end{aligned} \tag{20}$$

The coefficients $B_i(i = 1...18)$ are function of $z$ for inhomogeneous adhesive layer. Combining Eqs. (18) and (20), we can express the complementary energy functional of the system as:

$$\begin{aligned} \Pi = \pi \int_0^l \Big[ & (\alpha_1 + k^2 \alpha_2 + k\alpha_3)\ddot{\sigma}_1^2 + A_4 \sigma_1^2 + \alpha_4 \sigma_2^2 + B_5 \ddot{\sigma}_2^2 + (A_5 + k A_6)\sigma_1 \ddot{\sigma}_1 \\ & + \alpha_5 \dot{\sigma}_1^2 + \alpha_6 \sigma_2 \ddot{\sigma}_2 + (k\alpha_7 + \alpha_8)\sigma_2 \ddot{\sigma}_1 + (k B_8 + B_{10})\ddot{\sigma}_1 \ddot{\sigma}_2 \\ & + B_{16}\dot{\sigma}_2^2 + B_{18}\dot{\sigma}_1 \dot{\sigma}_2 \Big] \ dz \end{aligned} \tag{21}$$

where, the coefficients $\alpha_i(i = 1...8)$ are functions of $z$, akin to the coefficients $B_j$ and can be obtained by comparing Eqs. (18) and (20) with Eq. (21). The above functional is of the form:

$$\Pi(\sigma_1, \sigma_2, k) = \pi \int_0^l \varphi\Big(\sigma_1(z), \sigma_2(z), \dot{\sigma}_1(z), \dot{\sigma}_2(z), \ddot{\sigma}_1(z), \ddot{\sigma}_2(z), z, k\Big) dz \tag{22}$$

We adopt a variational method to obtain governing ODEs. Our task here is to determine the functions that minimize the functional $\Pi$. Here, $z$ is an independent variable and the integrand $\varphi$ depend on stress functions $(\sigma_1(z), \sigma_1(z))$ and their higher order derivatives as well as the unknown constant $k$. The extremal functions are solutions of the Euler–Lagrange equations that are obtained by setting the first variational derivatives of the functional with respect to each function equal to zero. Accordingly, we obtain a pair of coupled nonlinear ordinary differential equations (ODEs):

$$[M_{ij}]\begin{pmatrix} \ddot{\sigma}_1 \\ \ddot{\sigma}_2 \end{pmatrix} + [N_{ij}]\begin{pmatrix} \ddot{\sigma}_1 \\ \ddot{\sigma}_2 \end{pmatrix} + [P_{ij}]\begin{pmatrix} \dot{\sigma}_1 \\ \dot{\sigma}_2 \end{pmatrix} + [Q_{ij}]\begin{pmatrix} \dot{\sigma}_1 \\ \dot{\sigma}_2 \end{pmatrix} + [R_{ij}]\begin{pmatrix} \sigma_1 \\ \sigma_2 \end{pmatrix} = \begin{pmatrix} 0 \\ 0 \end{pmatrix} \tag{23}$$

where, the matrices $M_{ij}$, $N_{ij}$, $P_{ij}$, $Q_{ij}$, and $R_{ij}$ depend on the geometric and material properties of the bonded system as well as the loading condition. The elements of these matrices are function of $z$ and are given in the Appendix B. The indices $i$ and $j$ can range over 1–2. The optimal value of $k$ is determined by setting $\frac{\partial \Pi}{\partial k} = 0$. Accordingly, we get

$$\pi \int_0^l \left[ \left(2k\alpha_2(z) + \alpha_3(z)\right) \ddot{\sigma}_1^2 + A_6 \ \sigma_1 \ \ddot{\sigma}_1 + \alpha_7(z) \ \sigma_2 \ \ddot{\sigma}_1 + B_8(z) \ \ddot{\sigma}_1 \ \ddot{\sigma}_2 \right] dz = 0. \tag{24}$$

Coupled ODEs given by Eq. (23) and the integro-differential equation given by Eq. (24) can together be solved to determine the stress state in the assembly using the traction and traction-free boundary conditions given below.

$$\sigma_1(0) = 0; \quad \sigma_{rz}^{(1)}(r, 0) = 0; \quad \sigma_1(l) = \sigma_0; \quad \sigma_{rz}^{(1)}(r, l) = 0; \quad r \in [0, a] \tag{25}$$

$$\sigma_2(0) = 0; \quad \sigma_{rz}^{(2)}(r, 0) = 0; \quad \sigma_2(l) = 0; \quad \sigma_{rz}^{(2)}(r, l) = 0; \quad r \in [a, b] \tag{26}$$

### 2.2. Homogeneous adhesive layer

For the homogeneous adhesive layer, it is Young's modulus $E_2$ is constant over the embedment length. The coupled ODEs for this case become linear and are given as follows:

$$[\tilde{M}_{ij}]\begin{pmatrix} \ddot{\sigma}_1 \\ \ddot{\sigma}_2 \end{pmatrix} + [\tilde{N}_{ij}]\begin{pmatrix} \ddot{\sigma}_1 \\ \ddot{\sigma}_2 \end{pmatrix} + [\tilde{P}_{ij}]\begin{pmatrix} \dot{\sigma}_1 \\ \dot{\sigma}_2 \end{pmatrix} + [\tilde{Q}_{ij}]\begin{pmatrix} \dot{\sigma}_1 \\ \dot{\sigma}_2 \end{pmatrix} + [\tilde{R}_{ij}]\begin{pmatrix} \sigma_1 \\ \sigma_2 \end{pmatrix} = \begin{pmatrix} 0 \\ 0 \end{pmatrix} \tag{27}$$

where, the elements of the matrices $\tilde{M}_{ij}$, $\tilde{N}_{ij}$, $\tilde{P}_{ij}$, $\tilde{Q}_{ij}$, and $\tilde{R}_{ij}$ are constant. These matrices are obtained by setting derivatives of $z$ to zero in the matrices $M_{ij}$, $N_{ij}$, $P_{ij}$, $Q_{ij}$, and $R_{ij}$. The optimal value of $k$ for this case is determined from the following integro-differential equation

$$2k\,(\alpha_2 + \alpha_3) \int_0^l \ddot{\sigma}_1^2 \, dz + A_6 \int_0^l \sigma_1 \ddot{\sigma}_1 \, dz + \alpha_7 \int_0^l \sigma_2 \ddot{\sigma}_1 \, dz + B_8 \int_0^l \ddot{\sigma}_1 \ \ddot{\sigma}_2 \, dz = 0. \tag{28}$$

Note that $\alpha_2$, $\alpha_3$, $\alpha_7$, and $B_8$ become constant for this case.

## 3. Solution procedure

The set of governing equations (Eqs. (23) and (24) or Eqs. (27) and (28)) need to be simultaneously solved to get the actual solution for $\sigma_1$ and $\sigma_2$ which minimize the functional, imposing traction and traction-free boundary conditions given by Eqs. (25) and (26). However, we need to know $k$ from the integro-differential equations (Eq. (24) or Eq. (28)) in order to solve the pair of coupled ODEs. But $k$ can be evaluated only if we know the stress functions $\sigma_1$ and $\sigma_2$. Therefore, we initially find the approximate value of $k$ by fitting a cubic polynomial for the stress functions $\sigma_1$ and $\sigma_2$ since we know four boundary conditions for each of them. Accordingly, we initially impose

$$\sigma_1 = \sigma_0 \left(\frac{z}{l}\right)^2 \left[3 - 2\left(\frac{z}{l}\right)\right]; \qquad \sigma_2 = 0 \tag{29}$$

and solve the integro-differential to obtain the following initial approximate value for $k$ such that

$$k = \begin{cases} \dfrac{A_6 \frac{6\sigma_0^2}{5l} - \int_0^l \alpha_3 \left[36\sigma_0^2 \dfrac{\alpha_2(z)}{l^4}\left(1 - \dfrac{2z}{l}\right)^2\right] dz}{2\int_0^l \left[36\sigma_0^2 \dfrac{\alpha_2(z)}{l^4}\left(1 - \dfrac{2z}{l}\right)^2\right] dz}; & \text{if} \quad E_2 = E_2(z) \\ \dfrac{\left(A_6 \ l^2 - 10\alpha_3\right)}{20\alpha_2}; & \text{if} \quad E_2 = \text{Constant}. \end{cases}$$

This approximate value of $k$ is subsequently used together with BCs given by Eqs. (25) and (26) to find the solution for the coupled ODEs. Thus, we obtain approximate numerical solution for $\sigma_1$ and $\sigma_2$ and their derivatives over the entire embedment length. Now we use this solution set to evaluate a new value of $k$ solving the integro-differential (Eqs. 24 or (28)). Again we use the current value of $k$ to solve coupled ODEs. This process is repeated until the value of $k$ attains a constant value, i.e., $\left(k^j - k^{j-1}\right) \approx 0$. The converged $k^j$ is the optimal value and the $\sigma_1^{j-1}$ and $\sigma_2^{j-1}$ and their derivatives correspond to actual stress state. Once we know the actual distribution of $\sigma_1$ and $\sigma_2$ and their derivatives, we can determine the complete stress state in the entire system using the expressions for stress components derived in Section 2.

## 4. Homogeneous, tailored and degraded bondlayers

### 4.1. Bondlayer with tailored modulus over entire embedment length $l$

The homogeneous/non-tailored bondline (HBL) with Young's modulus $E_m$ $(=E_2)$ is considered as a baseline. The critical length required for complete shear stress-transfer for the system with homogeneous

adhesive modulus $E_m$ is $l_c$. In case of tailored bondline, the adhesive modulus is considered to vary as a function of the axial distance $z$ over the entire bondlength $l$ (Fig. 1). The following functional forms of modulus variation as shown in Fig. 6 are considered.

$$Ef_0 = E_0 \tag{30}$$

$$Ef_i = (E_0 - E_p)\left(\frac{z}{l}\right)^n + E_p \quad ; \qquad i = n = 1, 2, 3, 4 \tag{31}$$

$$Ef_5 = E_m \tag{32}$$

Eqs. (30) and (32) represent constant modulus profile for homogeneous compliant and stiff bondlines respectively, while Eq. (31) represents an inhomogeneous bondline whose modulus varies over the entire bondlength $l$ such that its value is $E_0$ at $z = l$ and $E_p$ at $z = 0$. Note that the effective modulus of the tailored bondline is enforced to be the same as the modulus of the homogeneous adhesive, $E_m$ and therefore

$$E_p = \frac{(n+1)}{n}\left[E_m - \frac{E_0}{(n+1)}\right] \quad ; \quad 0 < n < \infty \tag{33}$$

### 4.2. Degraded bondlayer

The adhesive is considered to have degraded over a fraction of bondlength $'\zeta l'$ from the loaded end of the anchor/fiber such that $0 < \zeta < 1$ as shown in Fig. 11. The adhesive is expected to degrade to a greater extent, due to higher stresses and faster degradation rate proximal to the loaded end. Therefore, we have chosen such a modulus profile. The adhesive modulus is constant over $0 \le z \le (1-\zeta)l$ and varies according to power law over $(1-\zeta)l \le z \le l$. The modulus profile of the adhesive in this case can be defined as

$$Ef_i = \begin{cases} E_m & ; \quad 0 \le z < (1-\zeta)l \\ (E_d - E_m)\left(\frac{z-(1-\zeta)l}{l\zeta}\right)^n + E_m & ; \quad (1-\zeta)l \le z \le l \end{cases} \tag{34}$$

where $0 \le \zeta \le 1$ and $n$ is a positive integer. Note that $0 < E_d < E_m$.

- If $\zeta \to 0$, then $Ef_i \to E_m$ representing a homogeneous stiff/intact adhesive according to first row of Eq. (34).
- If $\zeta \to 1$, then $Ef_i$ represents a bondline which is degraded over entire bondlength $l$ according to second row of Eq. (34).
- If $0 < \zeta < 1$, it represents a partially degraded bondline over length $\zeta l$ from the loaded end according to Eq. (34), see Fig. 11.

Solving governing equations for partially degraded bondline case with $Ef_i$ given by Eq. (34) is cumbersome and therefore a single profile for the adhesive modulus was constructed using a logistic growth function $\varrho(z)$. A logistic growth function $\varrho(z)$ is S-shaped (sigmoidal) curve that can be used to model functions that increase gradually at first, more rapidly in the middle, and slowly at the end, leveling off at a maximum value. A sigmoid function is given below for the degraded and intact regions of the bondline such that

$$\varrho(z) = \frac{1}{1 + e^{-\varsigma(z-(1-\zeta)l)}} \begin{cases} \varrho(z) = 0^+ & ; \quad \text{if } z < (1-\zeta)l \\ \varrho(z) = 1^- & ; \quad \text{if } z > (1-\zeta)l \end{cases} \tag{35}$$

where, $\varsigma$ dictates the steepness of the curve. $\varsigma > 0$ is chosen to control the gradient of the curve near $(1-\zeta)l$. From Eqs. (34) and (35), a continuous modulus profile for a partially degraded bondline can be written as

$$E_2(z) = (1-\varrho)E_m + \varrho\left((E_d - E_m)\left(\frac{z-(1-\zeta)l}{l\zeta}\right)^n + E_m\right) \tag{36}$$

## 5. Results and discussion

### 5.1. Homogeneous bondlayer (HBL)

For a bonded system with a homogeneous adhesive, considering the Young's modulus of the anchor $E_1$=210 GPa, Poisson's ratio of the anchor $\nu_1$=0.3, Young's modulus of the adhesive/matrix $E_2 = E_m$=3920 MPa, Poisson's ratio of the adhesive/matrix $\nu_2$=0.4, $l$=150 mm, $a$=5 mm, $b$=6 mm and $\sigma_0$=12.73 MPa, both theoretical results and 3D axisymmetric FE results are obtained. Henceforth, aforementioned properties are used unless otherwise stated.

The shear-lag solution, having relevance to many stress-transfer problems including the anchor problem here (and directly a single-fiber composite pullout problem), has a simplified closed-form solution as reviewed by Hull and Clyne (1996) and discussed by many authors including Kelly's early work on composites (Kelly and Tyson, 1965). The shear-lag solution which assumes no shear strain in the fiber and no transfer of normal stress across the fiber-end (Kelly and Tyson, 1965; Lawrence, 1972; Chua and Piggott, 1985), for the single-fiber pullout test gives following closed form expressions for the axial stress in the fiber $\sigma_{zz}^{(1)}$ and interfacial shear stress $\sigma_{rz}^{(2)}$:

$$\sigma_{zz}^{(1)} = \sigma_0\left(\frac{\sinh\left[\frac{qz}{a}\right]}{\sinh\left[\frac{ql}{a}\right]}\right) \tag{37}$$

$$\sigma_{rz}^{(2)} = \frac{q\sigma_0}{2}\left(\frac{\cosh\left[\frac{qz}{a}\right]}{\sinh\left[\frac{ql}{a}\right]}\right) \tag{38}$$

where, the dimensionless constant $q$ is given by,

$$q = \left[\frac{2G_2}{E_1}\frac{1}{\ln(\frac{b}{a})}\right]^{\frac{1}{2}} \tag{39}$$

Note that $\sigma_{zz}^{(1)}$ and $\sigma_{rz}^{(2)}$ predicted by the shear-lag model do not vary over the radial coordinate $r$. Fig. 2a and b shows the normalized axial stress in the anchor and normalized shear stress in the adhesive layer at the mid-surface of the adhesive layer respectively over the normalized embedment length ($\eta = \frac{z}{l}$). A good match between the analytical, shear-lag model (Lawrence, 1972; Chua and Piggott, 1985) and FE results validates the accuracy of the proposed theoretical model. For the geometric and material properties considered here, the critical length ($l_c$) required for the system with homogeneous adhesive of modulus $E_m$ is about 135 mm. In Fig. 2b the stress at the mid-surface of the adhesive layer is compared instead of comparing anchor-adhesive interface stress as the proposed analytical model does not capture the singular stress-field at the free surface of the bi-material interface. The proposed analytical model also satisfies the zero shear stress condition exactly at $z = l$ unlike the shear-lag solution. Fig. 3a and b shows the shear stress at different radial adhesive surfaces over the embedment length and the shear stress at different $z$ locations across the cross-section of the assembly, respectively. It can be seen from Fig. 3a and b that the peak shear stress occurs at the anchor-adhesive interface but close to the loaded end. Fig. 4a and b shows the shear stress distribution for three different thicknesses of adhesive layer over the embedment length at $r = a$ and at $r = (a+b)/2$ respectively. Fig. 4a and b confirms again that the peak shear stress always occurs at $r = a$ although the magnitude of peak shear stress decreases with increase in adhesive thickness as expected. Note that the increase in thickness of homogeneous adhesive does not warrant larger $l_c$. Fig. 5a and b shows the axial stress in the anchor and the shear stress distribution in the adhesive for different homogeneous adhesives at $r = a$, over the embedment length, respectively. Decrease in Young's modulus from 3290 MPa, warrants larger $l_c$ for shear-dominated stress-transfer. The discussion pertinent to pullout strength is based on shear stress failure criterion. It was considered that the crack would emanate from the

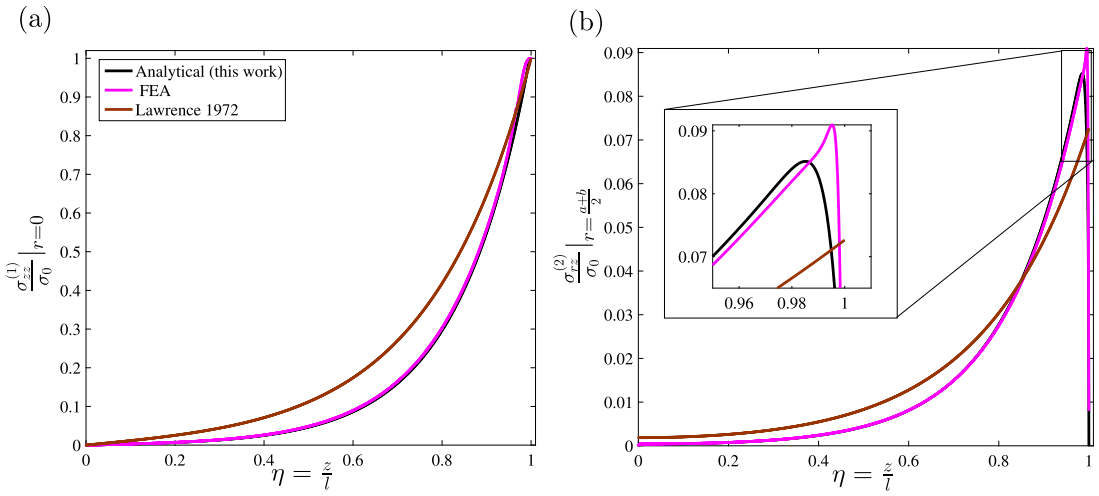


**Fig. 2.** HBL-Analytical vs FEA: a. Axial stress in the anchor over the embedment length and b. Shear stress at the mid-surface of the adhesive layer over the embedment length; the analytical solution is benchmarked with FE results and shear-lag solution (Lawrence, 1972).

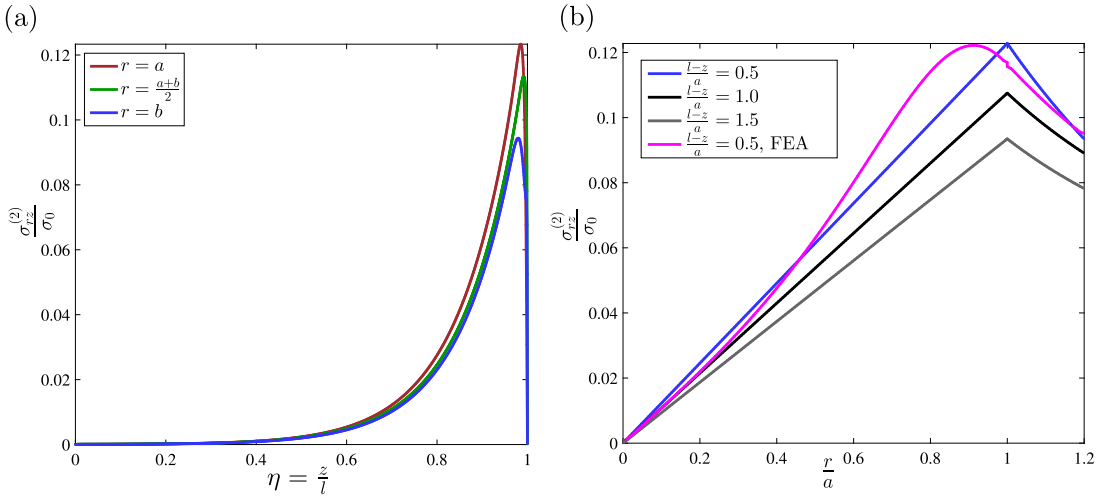


**Fig. 3.** HBL-Analytical: a. Shear stress at different radial surfaces of the adhesive layer over the embedment length and b. Shear stress across the cross section of axisymmetric bonded system at different $z$ locations.

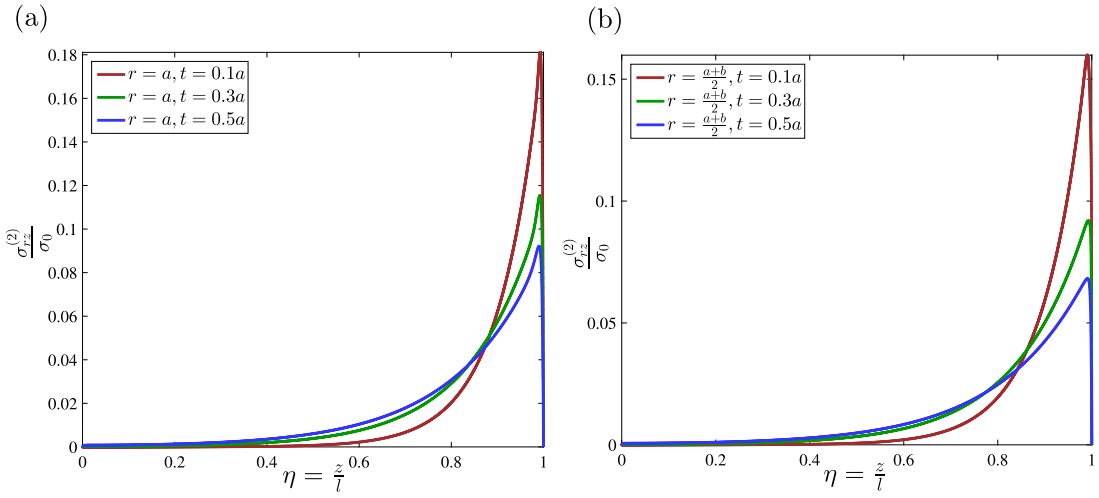


**Fig. 4.** HBL-Analytical: Adhesive shear stress over embedment length for different adhesive thicknesses. (a) Anchor-adhesive interface and (b) Mid-surface of the adhesive.

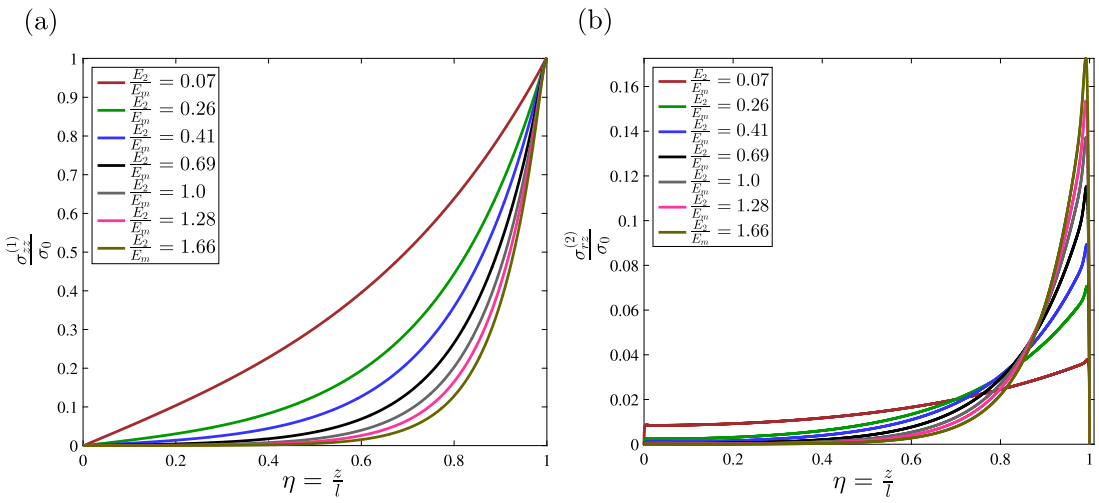


**Fig. 5.** HBL-Analytical: a. Axial stress in the anchor and b. Adhesive shear stress over embedment length at $r = a$ for different Young's moduli of the adhesive. Note, $E_m$ represents the identified modulus of the adhesive needed for shear-dominated load-transfer for the parameters chosen here.

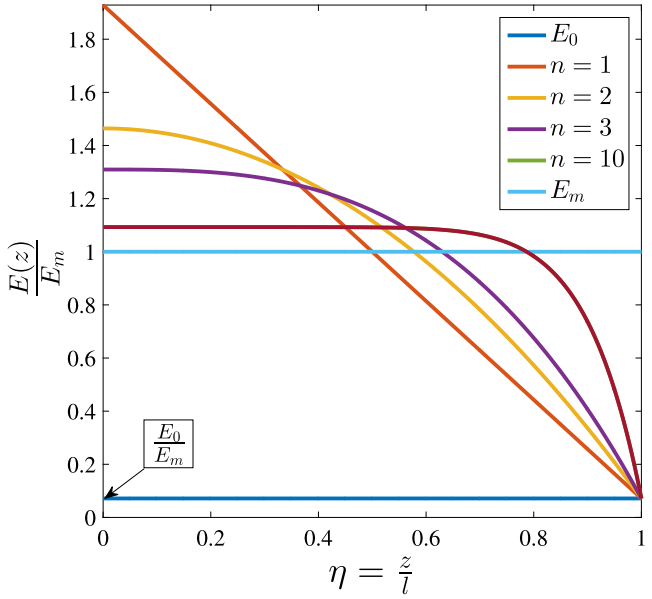


**Fig. 6.** Normalized modulus profiles for stiffness-tailored and homogeneous bondlines over entire embedment length $l$ for different values of $n$.

anchor-adhesive interface at the loaded end when the shear stress in the adhesive exceeds adhesive shear strength $\tau_c$ = 6.2 MPa (Prieto-Muñoz et al., 2010). For the range of embedment lengths considered here, always failure initiation in the adhesive is assumed to occur upon shear stress reaching a critical value at the loaded-end of the anchor.

### 5.2. Tailored bondlayer (TBL) over entire embedment length $l$

In this section, the adhesive modulus variation over the entire length $l$ is discussed in the context of material tailoring (see, Fig. 6) so as to improve the pullout performance. Adopting $Ef_2$ ($n$=2) with $E_0$= 280 MPa and using $E_p$ calculated from Eq. (33), analytical solution is obtained and compared with the 3D axisymmetric FE solution. In the FE model, variation of modulus is incorporated through a user defined subroutine called UMAT in Abaqus FEA. Fig. 7 shows the normalized shear stress over the normalized embedment length obtained both from analytical and FE models at the mid-surface of the adhesive layer for $l$=150 mm. Fig. 7 yet again demonstrates the accuracy of proposed theoretical model when a tailored bondline is considered. Incorporation of adhesive compliance proximal to the loaded-end of the anchor/fiber, reduces the peak shear stress by about 60% and the location of peak shear stress is slightly shifted away from the loaded-end of the anchor. Tailoring, besides reducing stress concentration, enables strain-tolerance of the composite system. This may increase the failure initiation threshold and has the potential for improving both strength and toughness properties of the bonded anchors simultaneously (Kumar et al., 2016).

Fig. 8a and 8b shows the axial stress in anchor and the shear stress distribution over the embedment length for various modulus profiles ($n$=1, 2, 3 and 10), respectively. $E_m$ and $E_0$ represent stiff and compliant homogeneous bondlines respectively. All of the tailored bondlines have the same effective modulus as that of stiff HBL ($E_m$). Therefore, all cases except for HBL with stiffness $E_0$ require the same $l_c$. $E_0$, being a compliant HBL, the embedment length $l$=150 mm is not sufficient for shear-dominated stress-transfer. By tailoring the bondline's stiffness, we could optimally redistribute the stresses in the adhesive layer over the embedment length without changing the global stiffness of the system. Fig. 8b clearly shows that the shear stress could be redistributed in a desired fashion by appropriately designing the modulus variation over the embedment length. Note that the peak shear stress is minimum for the case of a linearly-tailored adhesive.

Fig. 9 shows the shear stress distribution at the mid-surface of the adhesive layer over the embedment length for various embedment lengths for a modulus profile $Ef_1$ as a function of $\frac{E_0}{E_m}$ ratio. Fig. 9a is for $l < l_c$, Fig. 9b is for $l = l_c$ and Fig. 9c is for $l > l_c$. Stress distribution for each case is given for various tailored bondlines with same effective stiffness as that of HBL by changing the $E_0$. This allows us to choose an optimum $\frac{E_0}{E_m}$ ratio for a given $l$, $Ef_1$ and other geometric and material parameters. Note that for anchors with embedment length $l$ greater than $10a$ and tailored bondline with $\frac{E_0}{E_m} \leq 0.4$, the reduction in peak stress is dependent of embedment length. Note that the entire load $P$ is transferred to the concrete through shearing of lateral surface of the adhesive layer as the embedded-end is considered to be completely debonded/unbonded. Therefore, we can write:

$$P = 2\pi b \int_0^l \sigma_{rz}^{(2)}(b, z)\, dz \tag{40}$$

Fig. 9d shows the maximum shear stress in the adhesive layer as a function of $\frac{l}{a}$ for both graded and non-tailored interlayers. It can seen from Fig. 9d that the maximum shear stress in the adhesive layer for both cases decrease with increase in $l$ and saturates eventually. However, the maximum shear stress in the TBL is always less than

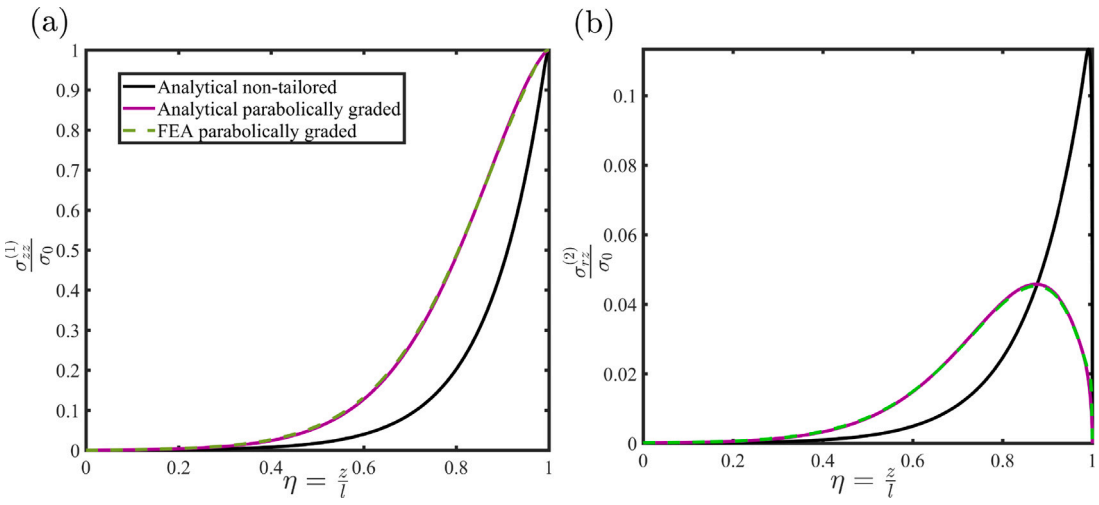


**Fig. 7.** TBL-Analytical Vs. FEA: a. Axial stress in the anchor and b. Shear stress distribution at the mid-surface of the adhesive layer for $Ef_2$ and $l = 150$ mm. Note that the peak shear stress decreases by 59.45%.

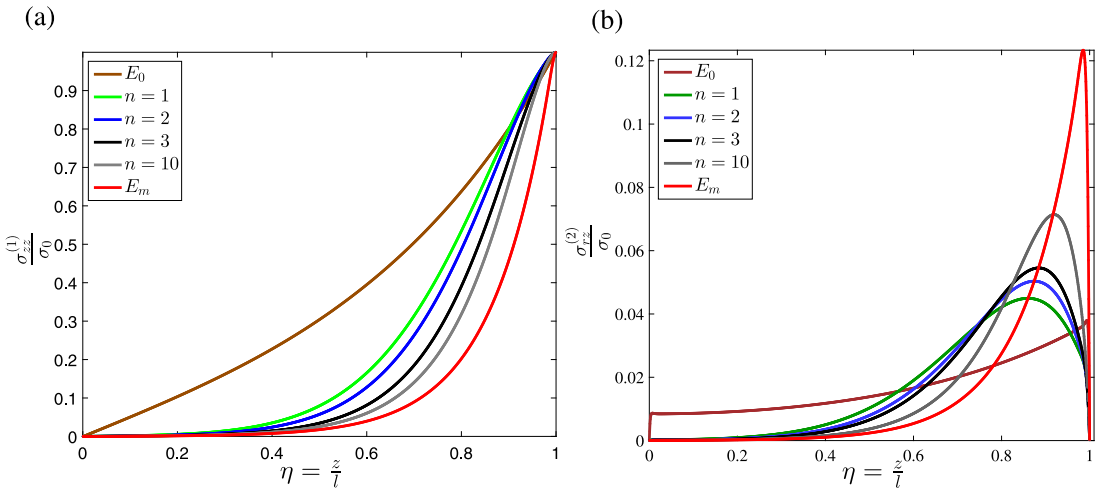


**Fig. 8.** TBL-Analytical: a. Axial stress in the anchor and b. Adhesive shear stress over embedment length, for different modulus profiles ($l = 150$ mm) compared with stiff and compliant HBLs. Note $l_{cr}$ is same for all except for HBL with modulus $E_0$.

the HBL. It can be observed that the optimum $l$ for both cases are different for the parameters considered here. From Fig. 9d for $l = 50a$, the maximum shear stress decreases by about 63% if a TBL is employed in lieu of a HBL. It also indicates that tailored bondline requires longer embedment length for complete shear stress-transfer.

Fig. 10a–c shows the shear stress distribution for different adhesive thicknesses for various $\frac{E_0}{E_m}$ ratios with $l$=150 mm and $E_{f1}$. Fig. 10d shows the maximum shear stress in the adhesive as a function of $\frac{t}{a}$ ratio for various $\frac{E_0}{E_m}$ ratios. Note that the maximum shear stress decreases by 35% for $t = 0.2a$. For the TBL, the shear strength of the adhesive is position dependent i.e., $\tau_c(z)$. When the maximum shear stress in TBL adhesive $\tau_{max}(z) \geq \tau_c(z)$, crack would initiate (Tipireddy and Kumar, 2017).

### 5.3. Degradation over partial length $\zeta l$

Considering bondline degradation over $\zeta l$ distance along $z$ from the loaded end, solutions were obtained using the analytical model adopting modulus profile given by Eq. (36) with $n = 1$ and $E_m$=3290 MPa and $E_d = \frac{E_m}{10}$ (Singer et al., 2018) under the same tensile load $P$ as before. As mentioned before, the factor $\zeta$ is chosen such that $0 < \zeta < 1$ to represent a bondline whose modulus has degraded over the length $\zeta l$ from the loaded end as shown in Fig. 11. Results were obtained for different choices of $\zeta$ for various embedment lengths $l$ under the same load and are presented in Fig. 12. For a given $l$, increasing $\zeta$, reduces the shear stress peak in the adhesive as larger fraction of bondline behaves in a compliant manner due to degradation. Reduction in peak shear stress is also accompanied by redistribution of shear stress over the embedment length to maintain equilibrium, warranting larger $l$ to enable shear-dominated stress-transfer. Fig. 12a shows the stress distribution for different choices of $\zeta$ for $l = 75$ mm. It is clear from this figure that $l = 75$ mm is not sufficient even for an intact bondline to completely transferring through shearing of the adhesive. However, the shear stress close to the embedded-end decays as the length is increased for a given value of $\zeta$ as shown in Figs. 12b–c. An important question from the view point of design of adhesive anchors when the bondline is partially degraded is whether the embedment length is sufficient for a shear-dominated load-transfer. In order to answer this question, a design map is generated by predicting shear stress distribution in the bondline for various embedment lengths but increasing the partial length over which the bondline has degraded. Shear stress-transfer length $l_c$ is computed such that complete shear transfer is regarded to

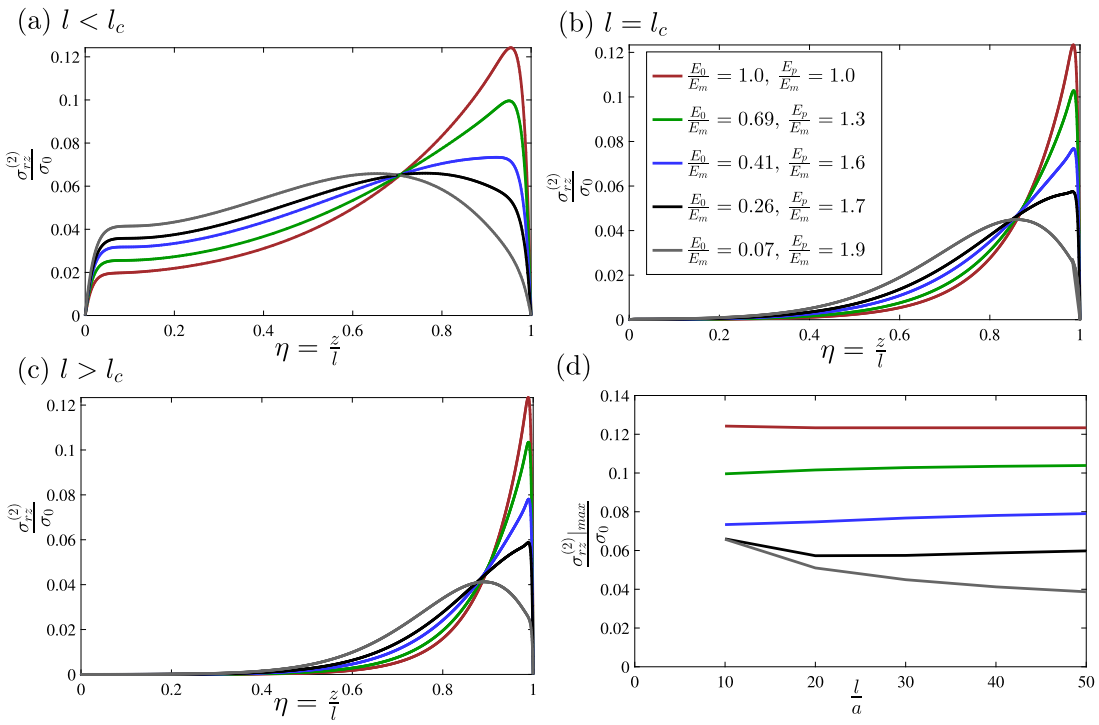


**Fig. 9.** TBL-Analytical: The shear stress distribution at the mid-surface of the adhesive as a function of embedment length $l$ along the bondline for $Ef_1$: (a) $l < l_c$; (b) $l = l_c$; (c) $l > l_c$; (d) Normalized maximum shear stress as a function of bondlength $l$ for linearly stiffness-tailored adhesive.

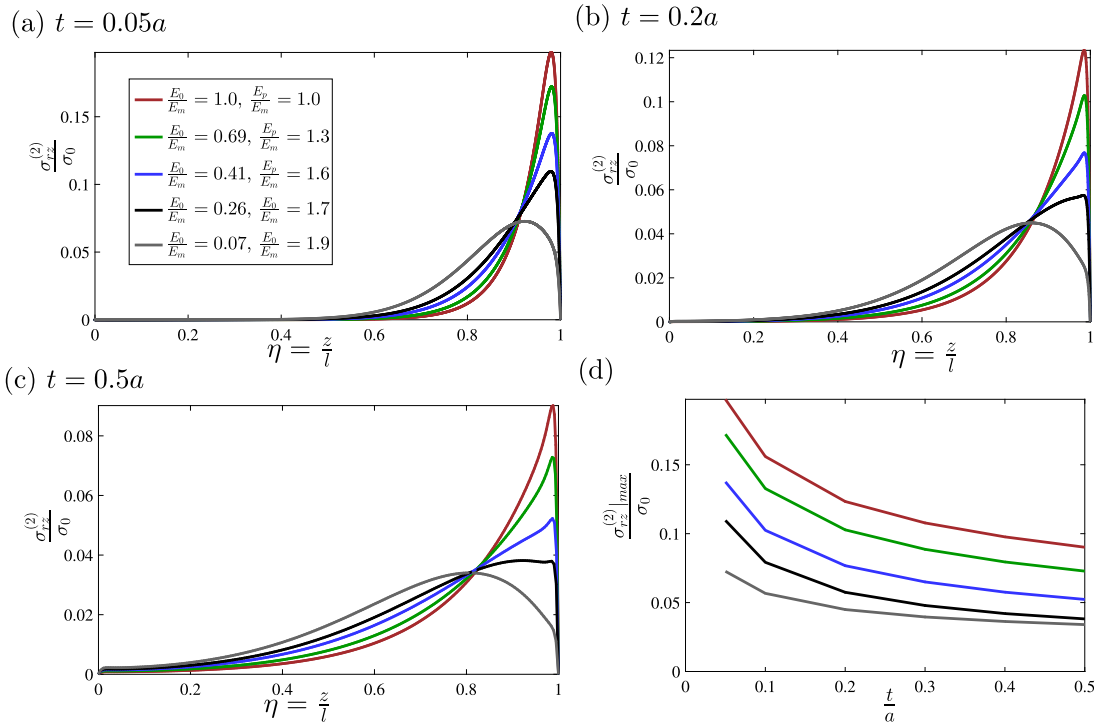


**Fig. 10.** TBL-Analytical: The shear stress distribution at the mid-surface of the adhesive for different $\frac{E_0}{E_m}$ ratios for $Ef_1$ and $l = 150$ mm. (a) $t = 0.05a$; (b) $t = 0.2a$; (c) $t = 0.5a$; (d) Normalized maximum shear stress as a function of adhesive thickness $t$.

have occurred when the area under shear stress curve dies down to less than 1% of total area under the shear stress curve over $z \leq 5\%l$ from the embedded-end of the anchor.

Fig. 13a shows the a design map clearly demarcating the regions where $l_c \leq l$ and $l_c \geq l$ for various choices of $l$, $\zeta$ and other geometric and material parameters. $\zeta$=0 indicates intact bondline while $\zeta$=1 indicates a bondline whose modulus is degraded over the entire length $l$. From Fig. 13a, one can see how degradation increases the shear stress-transfer-length required warranting larger embedment lengths. Fig. 13b shows the design map $\frac{l_c}{a}$ Vs. $\frac{\zeta l}{a}$ and gives the $l_c$ required as a function of degraded length of the bondlayer, for the parameters chosen here.

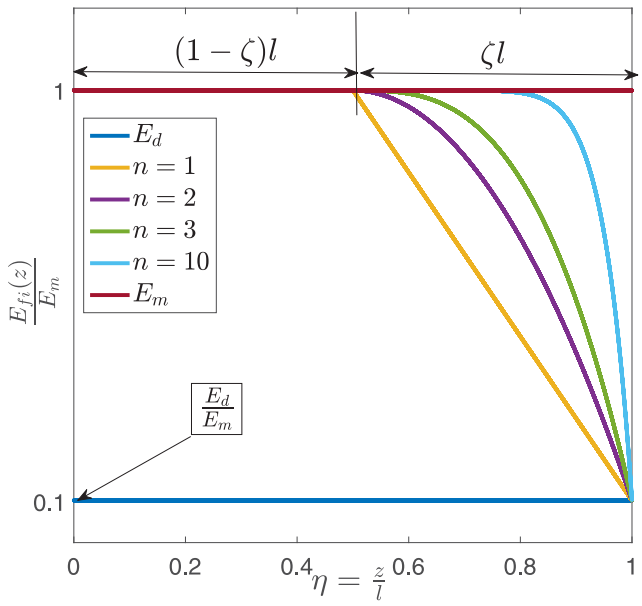


**Fig. 11.** Modulus profiles for partially deteriorated and homogeneous bondlines based on power law given by Eq. (36). Note, $\zeta$ varies such that $0 < \zeta < 1$.

Although Sections 5.2 and 5.3 focused on the elastic stresses in the tailored and degraded bondlines respectively, often, failure of the bonded anchors occurs due to the viscous nature of the adhesive. To capture the viscoelastic stresses in the adhesive, a variational method suitable for modeling dissipative systems (Pioletti and Rakotomanana, 2000; Vassoler et al., 2012) is required. Alternatively, Newtonian principles (equilibrium equations along with the viscoelastic constitutive laws) can be employed to predict the viscoelastic stresses in the adhesive (Shishesaz and Reza, 2013). Veisytabar et al. (2023) performed a viscoelastic analysis on bonded joints with tailored adherends, however, no studies have thus been reported for the case of bonded structural systems with graded adhesive; therefore, this aspect is suggested as a future study.

### 5.4. Interfacial fracture

Adhesively bonded anchors usually fail by one of the four possible failure modes as discussed in Section 1. It is envisaged that the failure of the bondlayer could occur in two possible ways viz. 1. interfacial fracture (adhesive failure) at anchor-adhesive interface and 2. cohesive failure of the bulk adhesive. Herein, the crack-growth resistance of the adhesive-anchor interface is modeled using J-integral method. The axisymmetric geometric and FE models with a pre-existing crack of length $\Gamma$ at the anchor-adhesive interface emanated from the loaded-end of anchor are shown in Fig. 14a and b respectively. In Fig. 14a, the interface crack is highlighted by a bold black line. The crack is modeled as a seam.

The virtual crack extension direction is specified with the $q$ vector. In the model shown in Fig. 14, $q$ vector is defined with the starting point at the crack tip and the end point at the red dot; the resulting $q$-vector is shown in red. Since, we consider a sharp interface crack, we have bi-material stress/strain singularity at the crack tip. We include the singularity at the crack tip so as to accurately calculate the J-integral and the stresses/strains. The partitioning of the geometry is defined by the circular line centered on the crack tip as shown in Fig. 14b. The crack tip is meshed using a ring of collapsed quadratic quadrilateral elements. Second-order elements are used to obtain a mesh singularity at the crack tip. The circular partitioned areas are meshed using the "swept meshing" technique; this method allows the mesh to be regular and focused. The remaining portion of the model is free meshed using the "medial axis" meshing algorithm. The edge-based tools for specifying mesh seeding facilitate the development of a focused mesh around the crack tip. The lateral adhesive-concrete interface is fully restrained to mimic the rigid concrete. ABAQUS FE code was used to perform the analysis. The variation in Young's modulus of the adhesive layer over the embedment length was implemented through a user defined subroutine called UMAT. As before, for inhomogeneous case $Ef_2$ is adopted with $E_m$ = 3920 MPa and $E_0$ = 280 MPa and for the homogeneous case $E_2$ = 3920 MPa.

Considering a crack of size $\Gamma$ at the anchor-adhesive interface at the loaded end, mode-II J-integral was evaluated for the linear-elastic system considering HBL, TBL and degraded bondline. The model is subjected to an axial ramping stress $\sigma_0$=100 MPa at loaded end of the anchor, while the debonded end is left free. Fig. 14c shows the energy release rate as a function of normalized interfacial crack length. Once shear crack initiates at the interface, Mode-II fracture along the anchor-adhesive interface might occur. For HBL, the fracture toughness $G_c^m$ is constant but the fracture toughness for the TBL $G_c^v$ is position dependent. For HBL, interface crack would grow if the energy release rate $G^m \geq G_c^m$ and for the TBL, crack would grow if $G^v(z) \geq G_c^v(z)$. It can be seen from Fig. 14c that the energy release rate for the stiffness-varying bondline anchors is much lower than that of the HBL anchors for any given interface crack length while all other parameters being the same. The crack-growth resistance of the bonded anchors with stiffness-varying bondline anchors is different from that of the HBL anchors as evidenced by Fig. 14c. When $\Gamma$=0.1 $l$, the crack-growth resistance changes by about 66% for the parameters considered here. Therefore, it can be concluded that an engineered bondline with spatially-varying stiffness along embedment length is more damage tolerant than the HBL anchors.

The fracture analysis of adhesive–adherend interface based on J-integral approach requires the presence of an initial crack. To accurately predict the crack initiation and/or propagation within the bulk adhesive and/or at the adhesive–adherend interface in bonded systems, another energy-based approach, known as cohesive zone modeling (CZM) is widely used (Khoramishad et al., 2010). The CZM approach employs a traction–separation law - a sub-set of bond–slip models (see, for instance Anyfantis and Tsouvalis, 2012; Zhu et al., 2009). Several studies utilized the bilinear CZM approach to model the failure behavior of conventional bonded systems neglecting the plasticity and rate-dependent behavior of the adhesive. For the tailored bonded system explored herein, the bondline could be treated as a series of infinitesimal adhesives with appropriate bond–slip parameters. This requires extensive experimental characterization of traction–separation parameters as a function of spatial co-ordinates. Furthermore, the inelastic and rate-dependent behavior of the adhesive during separation at failure can be captured using a trilinear (or trapezoidal) traction–separation law (Pisavadia et al., 2022) and is left to a subsequent study.

## 6. Conclusions

In this study, 3D axisymmetric elasticity solutions for pull-out stresses are presented and validated. Analytical solutions for two different cases are proposed: (1) bonded anchor with tailored bondlayer retaining its effective stiffness in order to ensure shear-dominated load-transfer, and (2) stiffness degraded bondlayer. For the latter case, we identified the critical bondlength required for shear-dominated load-transfer through the adhesive. Both theoretical and FE results indicate that the maximum shear stress in the bondlayer can be decreased over 60% by incorporating a graded bondlayer in lieu of a homogeneous bondlayer for the set of geometric and material properties considered here. The proposed theoretical model was also used to evaluate the influence of loss of bondlayer stiffness due to degradation. A parametric

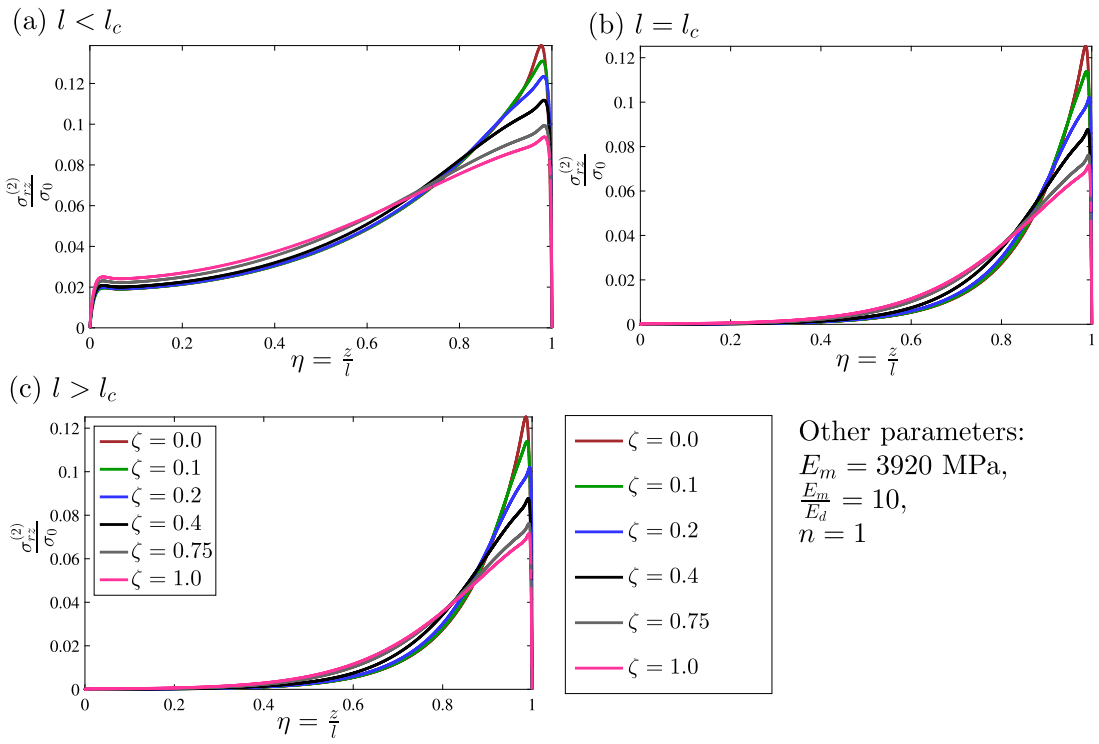


**Fig. 12.** Partially degraded bondline-Analytical: Shear stress distribution along the bondline at the mid-surface of the adhesive as a function of $\zeta$ for (a) $l < l_c$; (b) $l = l_c$; (c) $l > l_c$.

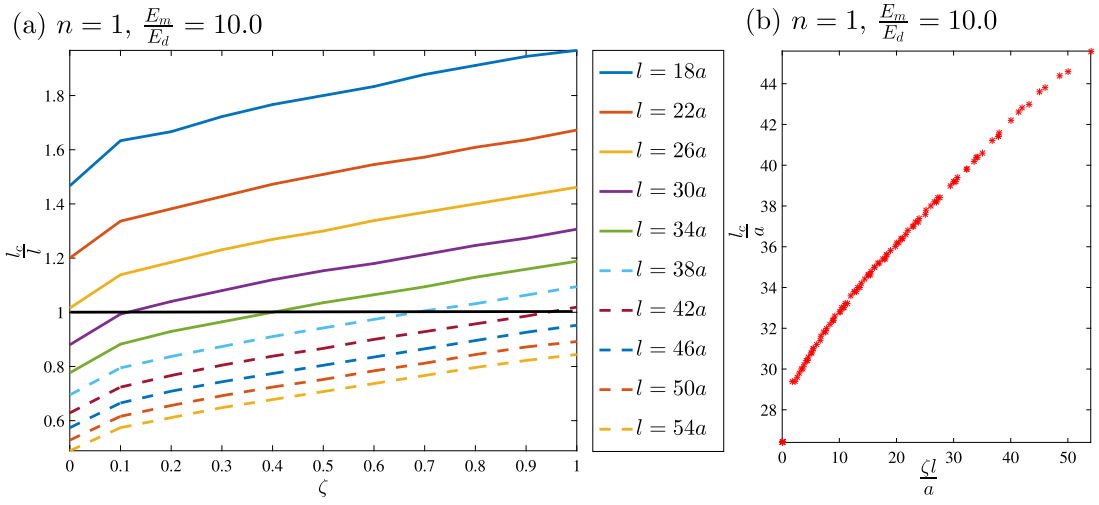


**Fig. 13.** Partially degraded bondline-Analytical: (a) Influence of $\zeta$ on shear stress-transfer length $l_c$ for various embedment lengths $l$ and (b) design map $\frac{l_c}{a}$ Vs. $\frac{\zeta l}{a}$.

study was conducted to study the effect of an inhomogeneous bondlayer on the interfacial stresses and crack growth resistance as a function of geometric and material properties of the anchorage system. Through fracture analyses of bonded anchors, it is concluded that an engineered or tailored bondlayer is more damage tolerant than anchors with homogeneous adhesive layer. This study also provides insights into the influence of loss of bondlayer stiffness on interfacial stresses and the design aspects of functionally graded and degraded adhesive anchors.

The following observations were made on the pull-out behavior of graded and degraded anchors:

- The linear tailoring of the bondline stiffness was found to be optimal from the perspective of peak stress reduction.
- For bonded anchors with embedment length greater than five times the diameter of anchor and tailored bondlayer with $\frac{E_0}{E_m} > 0.4$, the reduction in peak stress is independent of the embedment length.

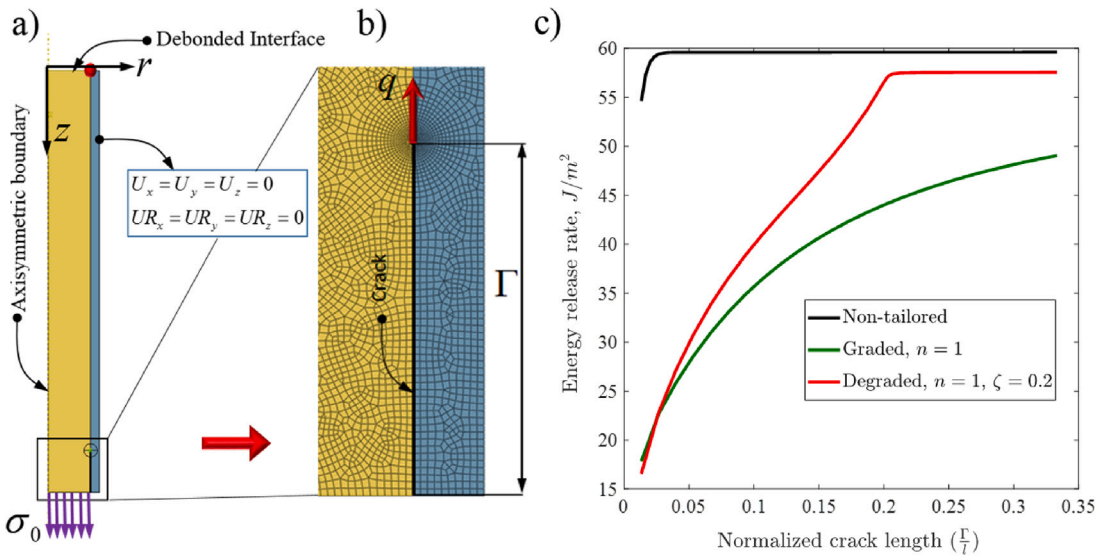


**Fig. 14.** A. Axisymmetric geometric model b. Axisymmetric FE model to simulate interfacial debonding at the anchor-adhesive interface from the loaded end of the anchor c. Energy release rate at the anchor-adhesive interface as a function of crack length.

- The reduction in peak shear stress is higher for the tailored anchor assemblies with larger embedment length and thinner adhesive.
- Anchors with larger embedment lengths can tolerate degradation of the bondlayer without warranting a larger critical shear-transfer-length.

This study only considered the elastic behavior of the adhesive layer and developed a theoretical framework to analyze pull-out stresses in the tailored and degraded adhesive anchors. However, failure of bonded anchors is often due to creep damage of the adhesive. A CZM approach capable of capturing the inelastic and viscous behavior of the adhesive could provide a robust modeling framework for accurately predicting the bond-failure and performance of functionally graded and degraded bonded systems.

## CRediT authorship contribution statement

**S. Kumar:** Conceptualization, Methodology, Validation, Formal analysis, Investigation, Resources, Writing – original draft, Writing - Review & Editing, Supervision. **M.A. Khan:** Software, Formal analysis, Investigation, Data curation, Writing – original draft, Writing – review & editing. **Brian L. Wardle:** Formal analysis, Investigation, Writing – original draft, Writing – review & editing. **J.N. Reddy:** Formal analysis, Investigation, Writing – original draft, Writing – review & editing.

## Declaration of competing interest

The authors declare that they have no known competing financial interests or personal relationships that could have appeared to influence the work reported in this paper.

## Data availability

No data was used for the research described in the article.

## Acknowledgments

S.K. would like to acknowledge the start-up grant provided by the University of Glasgow (Award No: 144690-1).

## Appendix A. Geometric and/or material properties

$$\xi = \frac{1}{(a-b)}\left(\frac{a^2}{4} + \frac{a^2}{2} ln\left(\frac{b}{a}\right)\right) \quad ; \quad \rho = \frac{1}{(a-b)}\frac{\nu_2}{1-\nu_2} \tag{A.1a}$$

$$\beta = \frac{1}{(a-b)}\left(\frac{a^2}{2} ln\left(\frac{b}{a}\right) + \frac{(a^2-b^2)}{4}\right) \tag{A.1b}$$

$$k_1 = \frac{2(1-\nu_1)}{E_1}; \quad k_2 = \frac{1}{E_1}; \quad k_3 = -4\frac{\nu_1}{E_1}; \quad k_4 = 2\frac{(1+\nu_1)}{E_1} \tag{A.1c}$$

$$A_1 = k_1 \int_0^a \frac{r^5}{16}\, dr\,; \quad A_2 = k_1 \int_0^a r\, dr\,; \quad A_3 = \frac{k_1}{2}\int_0^a r^3\, dr \tag{A.1d}$$

$$A_4 = k_2 \int_0^a r\, dr\,; \quad A_5 = k_3 \int_0^a \frac{r^3}{4}\, dr\,;$$
$$A_6 = k_3 \int_0^a r\, dr\,; \quad A_7 = -k_4 \int_0^a \frac{r^2}{2}\, dr \tag{A.1e}$$

## Appendix B. Geometric and/or material properties

$$\eta_1 = \frac{2(1-\nu_2)}{E_2(z)}, \quad \eta_2 = \frac{1}{E_2(z)}, \quad \eta_3 = -4\frac{\nu_2}{E_2(z)}, \quad \eta_4 = 2\frac{(1+\nu_2)}{E_2(z)} \tag{B.1a}$$

$$f_3 = \frac{(r-b)}{(a-b)}k, \quad f_4 = \frac{a^2}{2} ln\left(\frac{r}{b}\right) + \eta(r-b)\,; \quad f_5 = \rho(b-r) + \frac{\nu_2}{1-\nu_2} \tag{B.1b}$$

$$f_6 = \frac{a^2}{2} ln\left(\frac{b}{r}\right) + \frac{(r^2-b^2)}{4} + \beta(b-r) \tag{B.1c}$$

$$B_1 = \eta_1 \int_a^b f_3^2 r\, dr; \quad B_2 = \eta_1 \int_a^b f_4^2 r\, dr; \quad B_3 = 2\eta_1 \int_a^b f_3 f_4 r\, dr; \tag{B.1d}$$

$$B_4 = \eta_1 \int_a^b f_5^2 r\, dr; \quad B_5 = \eta_1 \int_a^b f_6^2 r\, dr; \quad B_6 = 2\eta_1 \int_a^b f_5 f_6 r\, dr; \tag{B.1e}$$

$$B_7 = 2\eta_1 \int_a^b f_3 f_5 r\, dr; \quad B_8 = 2\eta_1 \int_a^b f_3 f_6 r\, dr;$$
$$B_9 = 2\eta_1 \int_a^b f_4 f_5\, r\, dr; \quad B_{10} = 2\eta_1 \int_a^b f_4 f_6 r\, dr \tag{B.1f}$$

$$B_{11} = \eta_2 \int_a^b r dr; \quad B_{12} = \eta_3 \int_a^b f_3 r\, dr;$$

$$B_{13} = \eta_3 \int_a^b f_4 r\, dr; \quad B_{14} = \eta_3 \int_a^b f_5 r\, dr \tag{B.1g}$$

$$B_{15} = \eta_3 \int_a^b f_6 r\, dr; \quad B_{16} = \eta_4 \int_a^b f_7^2 r\, dr;$$
$$B_{17} = \eta_4 \int_a^b f_8^2 r\, dr; \quad B_{18} = 2\eta_4 \int_a^b f_7 f_8 r\, dr \tag{B.1h}$$

### B.1. Matrices

$$[M_{ij}] = \begin{bmatrix} 2\big(\alpha_1(z) + k^2\alpha_2(z) + k\alpha_3(z)\big) & kB_8(z) + B_{10}(z) \\ kB_8(z) + B_{10}(z) & 2B_5(z) \end{bmatrix} \tag{B.2}$$

$$[N_{ij}] = \begin{bmatrix} 2\big(\dot\alpha_1(z) + k^2\dot\alpha_2(z) + k\dot\alpha_3(z)\big) & 2\big(k\dot B_8(z) + \dot B_{10}(z)\big) \\ 2\big(k\dot B_8(z) + \dot B_{10}(z)\big) & 4\dot B_5 \end{bmatrix} \tag{B.3}$$

$$[P_{ij}] = \begin{bmatrix} 2(\ddot\alpha_1 + k^2\ddot\alpha_2 + k\ddot\alpha_3) + 3(A_5 + kA_6) - 2\alpha_5 & (k\alpha_7 + \alpha_8) + (k\ddot B_8 + \ddot B_{10}) - B_{18} \\ (k\alpha_7 + \alpha_8) + (k\ddot B_8 + \ddot B_{10}) - B_{18} & 2(\ddot B_5 + \alpha_6 - B_{16}) \end{bmatrix} \tag{B.4}$$

$$[Q_{ij}] = \begin{bmatrix} -2\dot\alpha_5 & 2(k\dot\alpha_7 + \dot\alpha_8) - \dot B_{18} \\ -\dot B_{18} & 2(\dot\alpha_6 - \dot B_{16}) \end{bmatrix} \tag{B.5}$$

$$[R_{ij}] = \begin{bmatrix} 2A_4 & (k\ddot\alpha_7 + \ddot\alpha_8) \\ 0 & (2\alpha_4 + \ddot\alpha_6) \end{bmatrix} \tag{B.6}$$

## Appendix C. Errata

$$\sigma_{rz}^{(2)}|_{z=l} = \frac{q\sigma_0}{2}\left(\frac{\cosh\left[\frac{ql}{a}\right]}{\sinh\left[\frac{ql}{a}\right]}\right); \quad q = \left[\frac{2G_2}{E_1}\frac{1}{\ln(\frac{b}{a})}\right]^{\frac{1}{2}} \tag{C.1}$$

let $k = \sqrt{\frac{2G_2}{E_1}}$, $x = \frac{1}{\sqrt{\ln(b/a)}}$

$$\sigma_{rz}^{(2)}|_{z=l} = \frac{k\sigma_0}{2} x \coth\left(\frac{kl}{a}x\right) \tag{C.2}$$

$$= \frac{k\sigma_0}{2} x \left(\frac{e^{\left(\frac{kl}{a}x\right)} + e^{\left(-\frac{kl}{a}x\right)}}{e^{\left(\frac{kl}{a}x\right)} - e^{\left(-\frac{kl}{a}x\right)}}\right) \tag{C.3}$$

$$= \frac{k\sigma_0}{2} x \left(\frac{1 + e^{\left(-2\frac{kl}{a}x\right)}}{1 - e^{\left(-2\frac{kl}{a}x\right)}}\right) \tag{C.4}$$

Using L. Hospital's rule,

$$= \frac{k\sigma_0}{2}\left(\frac{1 + e^{\left(-2\frac{kl}{a}x\right)} + x\, e^{\left(-\frac{2kl}{a}x\right)}\left(-\frac{2kl}{a}\right)}{\left(\frac{2kl}{a}\right)e^{\left(-\frac{2kl}{a}x\right)}}\right) \tag{C.5}$$

Applying L Hospitals rule again,

$$\sigma_{rz}^{(2)}|_{z=l} = \frac{k\sigma_0}{2}\left(\frac{e^{\left(-2\frac{kl}{a}x\right)}\left(-\frac{4kl}{a}x\right) + x\, e^{\left(-\frac{2kl}{a}x\right)}\left(\frac{2kl}{a}\right)^2}{-\left(\frac{2kl}{a}\right)^2 e^{\left(-\frac{2kl}{a}x\right)}}\right) \tag{C.6}$$

$$= \frac{k\sigma_0}{2}\left(\frac{a}{kl} - x\right) \tag{C.7}$$

Therefore, in limit sense

$$\lim_{x\to 0}\sigma_{rz}^{(2)}|_{z=l} = \frac{\sigma_0}{2}\frac{a}{l} \tag{C.8}$$

$$\lim_{x\to\infty}\sigma_{rz}^{(2)}|_{z=l} = -\infty \tag{C.9}$$

## References


Anyfantis, Konstantinos N., Tsouvalis, Nicholas G., 2012. A novel traction–separation law for the prediction of the mixed mode response of ductile adhesive joints. Int. J. Solids Struct. (ISSN: 0020-7683) 49 (1), 213–226. http://dx.doi.org/10.1016/j.ijsolstr.2011.10.001, URL https://www.sciencedirect.com/science/article/pii/S0020768311003313.

Ballarini, R., Shah, S.P., Keer, L.M., 1986. Failure characteristics of short anchor bolts embedded in a brittle material. Proc. R. Soc. Lond. Ser. A Math. Phys. Eng. Sci. 404 (1826), 35–54.

Bouchikhi, A.S., Lousdad, A., Megueni, A., 2010. On the reduce of interfacial shear stresses in fiber reinforced polymer plate retrofitted concrete beams. Mater. Des. 31 (3), 1508–1515.

Chen, Jianhang, Saydam, Serkan, Hagan, Paul C., 2015. An analytical model of the load transfer behavior of fully grouted cable bolts. Constr. Build. Mater. (ISSN: 0950-0618) 101, 1006–1015. http://dx.doi.org/10.1016/j.conbuildmat.2015.10.099, URL http://www.sciencedirect.com/science/article/pii/S0950061815305201.

Chua, P.S., Piggott, M.R., 1985. The glass fibre—polymer interface: I—theoretical consideration for single fibre pull-out tests. Compos. Sci. Technol. 22 (1), 33–42.

Cook, Ronald A., 1993. Behavior of chemically bonded anchors. J. Struct. Eng. 119 (9), 2744–2762.

Cook, R.A., Doerr, G.T., Klingner, R.E., 1993. Bond stress model for design of adhesive anchors. ACI Struct. J. 90 (5).

Cook, Ronald A., Konz, Robert C., 2001. Factors influencing bond strength of adhesive anchors. ACI Struct. J. 98 (1).

Cox, H.L., 1952. The elasticity and strength of paper and other fibrous materials. Br. J. Appl. Phys. 3 (3), 72.

Dadian, Alireza, Rahnama, Saeed, 2021. Experimental and numerical study of optimum functionally graded Aluminum/GFRP adhesive lap shear joints using Epoxy/CTBN. Int. J. Adhes. Adhes. (ISSN: 0143-7496) 107, 102854. http://dx.doi.org/10.1016/j.ijadhadh.2021.102854, URL https://www.sciencedirect.com/science/article/pii/S014374962100052X.

Doerr, G.T., Klingner, R., 1989. Adhesive Anchors: Load-Deflection Behavior and Spacing Requirements. University of Texas At Austin: Center for Transportation Research.

Durodola, J.F., 2017. Functionally graded adhesive joints–A review and prospects. Int. J. Adhes. Adhes.

Farmer, I.W., 1975. Stress distribution along a resin grouted rock anchor. Int. J. Rock Mech. Min. Sci. Geomech. Abstr. (ISSN: 0148-9062) 12 (11), 347–351. http://dx.doi.org/10.1016/0148-9062(75)90168-0, URL http://www.sciencedirect.com/science/article/pii/0148906275901680.

Gesoğlu, Mehmet, Güneyisi, Esra Mete, Güneyisi, Erhan, Yılmaz, Muhammet Enes, Mermerdaş, Kasım, 2014. Modeling and analysis of the shear capacity of adhesive anchors post-installed into uncracked concrete. Composites B 60, 716–724.

Hull, Derek, Clyne, T.W., 1996. An Introduction to Composite Materials. Cambridge University Press.

Kalfat, R., Al-Mahaidi, R., 2015. Finite element investigation into the size effect of bidirectional fibre patch anchors used to enhance the performance of FRP-to-concrete joints. Compos. Struct. 121, 27–36.

Kelly, A., Tyson, amd W.R., 1965. Tensile properties of fibre-reinforced metals: copper/tungsten and copper/molybdenum. J. Mech. Phys. Solids 13 (6), 329in1339–338in2350.

Khan, M.A., Kumar, S., 2018. Performance enhancement of tubular multilayers via compliance-tailoring: 3D printing, testing and modeling. Int. J. Mech. Sci. 140, 93–108.

Khan, M.A., Kumar, S., Reddy, J.N., 2018. Material-tailored adhesively bonded multilayers: A theoretical analysis. Int. J. Mech. Sci. 148, 246–262.

Khan, M.A., Wardle, B.L., Kumar, S., 2022. Elastic solutions for stresses in compliance-tailored adhesive anchors. Int. J. Adhes. Adhes. (ISSN: 0143-7496) 118, 103227. http://dx.doi.org/10.1016/j.ijadhadh.2022.103227, URL https://www.sciencedirect.com/science/article/pii/S0143749622001440.

Khoramishad, H., Crocombe, A.D., Katnam, K.B., Ashcroft, I.A., 2010. Predicting fatigue damage in adhesively bonded joints using a cohesive zone model. Int. J. Fatigue (ISSN: 0142-1123) 32 (7), 1146–1158. http://dx.doi.org/10.1016/j.ijfatigue.2009.12.013, URL https://www.sciencedirect.com/science/article/pii/S0142112309003648.

Kim, Myong-Ho, Hong, Hyon-Sik, Kim, Yong-Chol, 2021. Determination of failure envelope of functionally graded adhesive bonded joints by using mixed mode continuum damage model and response surface method. Int. J. Adhes. Adhes. (ISSN: 0143-7496) 106, 102815. http://dx.doi.org/10.1016/j.ijadhadh.2021.102815, URL https://www.sciencedirect.com/science/article/pii/S0143749621000130.

Kim, Yail J., LaBere, Jared, Yoshitake, Isamu, 2013. Hybrid epoxy-silyl modified polymer adhesives for CFRP sheets bonded to a steel substrate. Composites B 51, 233–245.

Kim, Seo Jin, Smith, Scott T., 2010. Pullout strength models for FRP anchors in uncracked concrete. J. Compos. Constr. 14 (4), 406–414. http://dx.doi.org/10.1061/(ASCE)CC.1943-5614.0000097, URL https://ascelibrary.org/doi/abs/10.1061/(ASCE)CC.1943-5614.0000097.

Kränkel, T., Lowke, D., Gehlen, C., 2015. Prediction of the creep behaviour of bonded anchors until failure–A rheological approach. Constr. Build. Mater. 75, 458–464.

Krasucki, Françoise, Lenci, Stefano, 2000. Analysis of interfaces of variable stiffness. Int. J. Solids Struct. 37 (26), 3619–3632.

Kumar, S., Adams, Robert D., 2017. Special issue on functionally graded adhesively bonded systems. Int. J. Adhes. Adhes. 76, 1–2.

Kumar, S., Khan, M.A., 2016a. An elastic solution for adhesive stresses in multi-material cylindrical joints. Int. J. Adhes. Adhes. 64, 142–152.

Kumar, S., Khan, M.A., 2016b. A shear-lag model for functionally graded adhesive anchors. Int. J. Adhes. Adhes. 68, 317–325.

Kumar, Shanmugam, Wardle, Brian L., Arif, Muhamad F., 2016. Strength and performance enhancement of bonded joints by spatial tailoring of adhesive compliance via 3D printing. ACS Appl. Mater. Interfaces.

Kumar, Shanmugam, Wardle, Brian L, Arif, Muhamad F, Ubaid, Jabir, 2018. Stress reduction of 3D printed compliance-tailored multilayers. Adv. Eng. Mater. 20 (1), 1700883.

Lawrence, P., 1972. Some theoretical considerations of fibre pull-out from an elastic matrix. J. Mater. Sci. 7 (1), 1–6.

Marques, J.B., Barbosa, A.Q., da Silva, C.I., Carbas, R.J.C., da Silva, L.F.M., 2021. An overview of manufacturing functionally graded adhesives – Challenges and prospects. J. Adhes. 97 (2), 172–206. http://dx.doi.org/10.1080/00218464.2019.1646647.

McCartney, L.N., 1989. New theoretical model of stress transfer between fibre and matrix in a uniaxially fibre-reinforced composite. Proc. R. Soc. Lond. Ser. A Math. Phys. Eng. Sci. 425 (1868), 215–244, The Royal Society.

McVay, Michael, Cook, Ronald A., Krishnamurthy, Kailash, 1996. Pullout simulation of postinstalled chemically bonded anchors. J. Struct. Eng. 122 (9), 1016–1024.

Nairn, John A., 1997. On the use of shear-lag methods for analysis of stress transfer in unidirectional composites. Mech. Mater. 26 (2), 63–80.

NTSB, 2007. Ceiling Collapse in the Interstate 90 Connector Tunnel Boston Massachusetts, July 10, 2006. Tech. Rep.

Paroissien, Eric, da Silva, Lucas F.M., Lachaud, Frédéric, 2018. Simplified stress analysis of functionally graded single-lap joints subjected to combined thermal and mechanical loads. Compos. Struct. (ISSN: 0263-8223) 203, 85–100. http://dx.doi.org/10.1016/j.compstruct.2018.07.015, URL https://www.sciencedirect.com/science/article/pii/S0263822318316891.

Pioletti, Dominique P., Rakotomanana, Lalao R., 2000. Non-linear viscoelastic laws for soft biological tissues. Eur. J. Mech. A Solids (ISSN: 0997-7538) 19 (5), 749–759. http://dx.doi.org/10.1016/S0997-7538(00)00202-3, URL https://www.sciencedirect.com/science/article/pii/S0997753800002023.

Pisavadia, Harshil, Toussaint, Geneviève, Dolez, Patricia, Hogan, James D, 2022. Cohesive zone failure modeling of polymeric adhesives used in ceramic/metal armor. Int. J. Impact Eng. 170, 104364.

Prieto-Muñoz, Pablo A., Yin, Huiming M., Testa, Rene B., 2010. An elastic analysis that predicts the pull-out capacity of adhesive anchors. In: IOP Conference Series: Materials Science and Engineering, Vol. 10. IOP Publishing, 012151.

Prieto-Muñoz, Pablo A., Yin, Huiming M., Testa, Rene B., 2013a. Mechanics of an adhesive anchor system subjected to a pullout load. I: Elastic analysis. J. Struct. Eng.

Prieto-Muñoz, Pablo A., Yin, Huiming M., Testa, Rene B., 2013b. Mechanics of an adhesive anchor system subjected to a pullout load. II: Viscoelastic analysis. J. Struct. Eng. 140 (2).

Rizzoni, Raffaella, Lebon, Frédéric, 2013. Imperfect interfaces as asymptotic models of thin curved elastic adhesive interphases. Mech. Res. Commun. 51, 39–50.

Sekiguchi, Y., Nakanouchi, M., Haraga, K., Takasaki, I., Sato, C., 2019. Experimental investigation on strength of stepwise tailored single lap adhesive joint using second-generation acrylic adhesive via shear and low-cycle shear tests. Int. J. Adhes. Adhes. (ISSN: 0143-7496) 95, 102438. http://dx.doi.org/10.1016/j.ijadhadh.2019.102438, URL https://www.sciencedirect.com/science/article/pii/S0143749619301873.

Shishesaz, Mohammad, Reza, Arash, 2013. The effect of viscoelasticity of adhesives on shear stress distribution in a double-lap joint using analytical method. J. Adhes. Sci. Technol. 27 (20), 2233–2250. http://dx.doi.org/10.1080/01694243.2013.769085.

Singer, G, Sinn, G, Schwendtner, K, Lichtenegger, H.C., Wan-Wendner, Roman, 2018. Time-dependent changes of mechanical properties of polymer-based composite materials for adhesive anchor systems. Compos. Struct. 196, 155–162.

Stapleton, Scott E., Najafian, Sara, Cassano, Alessandro, Schmidt, Daniel, 2021. Characterization of functionally graded adhesives using radiation curing. In: AIAA Scitech 2021 Forum. http://dx.doi.org/10.2514/6.2021-1403, URL https://arc.aiaa.org/doi/abs/10.2514/6.2021-1403.

Stapleton, Scott E., Waas, Anthony M., Arnold, Steven M., 2012. Functionally graded adhesives for composite joints. Int. J. Adhes. Adhes. 35, 36–49.

Steen, M., Valles, J.L., 1998. Interfacial bond conditions and stress distribution in a two-dimensionally reinforced brittle-matrix composite. Compos. Sci. Technol. 58 (3), 313–330.

Stein, N., Felger, J., Becker, W., 2017. Analytical models for functionally graded adhesive single lap joints: A comparative study. Int. J. Adhes. Adhes. 76, 70–82.

Tipireddy, R., Kumar, S., 2017. Spatially-degraded adhesive anchors under material uncertainty. Int. J. Adhes. Adhes. 76, 61–69.

Ubaid, Jabir, Wardle, Brian L., Kumar, Shanmugam, 2018. Strength and performance enhancement of multilayers by spatial tailoring of adherend compliance and morphology via multimaterial jetting additive manufacturing. Sci. Rep. 8 (1), 1–10.

Upadhyaya, Priyank, Kumar, S., 2015a. Micromechanics of stress transfer through the interphase in fiber-reinforced composites. Mech. Mater. 89, 190–201.

Upadhyaya, Priyank, Kumar, S., 2015b. Pull-out capacity of adhesive anchors: an analytical solution. Int. J. Adhes. Adhes. 60, 54–62.

Vassoler, J.M., Reips, L., Fancello, E.A., 2012. A variational framework for fiber-reinforced viscoelastic soft tissues. Internat. J. Numer. Methods Engrg. 89 (13), 1691–1706. http://dx.doi.org/10.1002/nme.3308, URL https://onlinelibrary.wiley.com/doi/abs/10.1002/nme.3308.

Veisytabar, Mehdi, Reza, Arash, Shekari, Younes, 2023. Stress analysis of adhesively-bonded single stepped-lap joints with functionally graded adherends based on the four-parameter fractional viscoelastic model. Eur. J. Mech. A Solids (ISSN: 0997-7538) 98, 104907. http://dx.doi.org/10.1016/j.euromechsol.2022.104907, URL https://www.sciencedirect.com/science/article/pii/S0997753822003370.

Wang, Yan-Jie, Wu, Zhi-Min, Zheng, Jian-Jun, Yu, Rena C., Zhou, Xiang-Ming, 2020. Three-dimensional axisymmetric analytical method for pull-out behaviour of adhesive anchors in concrete. Eng. Fract. Mech. (ISSN: 0013-7944) 226, 106876. http://dx.doi.org/10.1016/j.engfracmech.2020.106876, URL http://www.sciencedirect.com/science/article/pii/S0013794419311270.

Wu, W., Jacobs, Edgard, Verpoest, Ignace, Varna, Janis, 1999. Variational approach to the stress-transfer problem through partially debonded interfaces in a three-phase composite. Compos. Sci. Technol. 59 (4), 519–535.

Wu, W., Verpoest, Ignace, Varna, Janis, 1998. A novel axisymmetric variational analysis of stress transfer into fibres through a partially debonded interface. Compos. Sci. Technol. 58 (12), 1863–1877.

Yang, Shutong, Wu, Zhimin, Hu, Xiaozhi, Zheng, Jianjun, 2008. Theoretical analysis on pullout of anchor from anchor–mortar–concrete anchorage system. Eng. Fract. Mech. 75 (5), 961–985.

Zavliaris, K.D., Kollias, S., Speare, P.R.S., 1996. An experimental study of adhesively bonded anchorages in concrete. Mag. Concr. Res. 48 (175), 79–93.

Zhu, Yong, Liechti, Kenneth M., Ravi-Chandar, K., 2009. Direct extraction of rate-dependent traction–separation laws for polyurea/steel interfaces. Int. J. Solids Struct. (ISSN: 0020-7683) 46 (1), 31–51. http://dx.doi.org/10.1016/j.ijsolstr.2008.08.019, URL https://www.sciencedirect.com/science/article/pii/S0020768308003351.